

On the Whitham equations for the defocusing nonlinear Schrödinger equation with step initial data

Gino Biondini^{*} and Yuji Kodama[†]

^{*}: *State University of New York at Buffalo, Department of Mathematics, Buffalo, NY 14260*

[†]: *Ohio State University, Department of Mathematics, Columbus, OH 43210*

May 9, 2019

Abstract

The behavior of solutions of the finite-genus Whitham equations for the weak dispersion limit of the defocusing nonlinear Schrödinger equation is investigated analytically and numerically for piecewise-constant initial data. In particular, the dynamics of constant-amplitude initial conditions with one or more frequency jumps (i.e., piecewise linear phase) are considered. It is shown analytically and numerically that, for finite times, regions of arbitrarily high genus can be produced; asymptotically with time, however, the solution can be divided into expanding regions which are either of genus-zero, genus-one or genus-two type, their precise arrangement depending on the specifics of the initial datum given. This behavior should be compared to that of the Korteweg-de Vries equation, where the solution is divided into the regions which are either genus-zero or genus-one asymptotically. Finally, the potential application of these results to the generation of short optical pulses is discussed: the method proposed takes advantage of nonlinear compression via appropriate frequency modulation, and allows control of both the pulse amplitude and its width, as well as the distance along the fiber at which the pulse is produced.

The weak dispersion limit of the defocusing nonlinear Schrödinger (NLS) equation has been extensively studied in recent years (see e.g., Refs. [13, 22, 27, 29, 31]), and in some sense it is well-characterized mathematically. Not as much is known, however, about the detailed behavior of the solutions for specific choices of initial datum^[9, 10, 14, 25]. The purpose of this work is to present analytical and numerical results regarding the behavior of a special class of solutions of the NLS equation in the weak dispersion limit. More precisely, we consider the initial value problem for the NLS equation in the weak dispersion limit with the initial data having a constant-amplitude and piecewise constant frequency. We believe that, on one hand, this behavior is interesting mathematically, and that, on the other hand, it could have potential applications in the generation of intense, ultra-short optical pulses. As such, it is worthy of further study.

The structure of this document is as follows: in section 1 we introduce the problem, and in section 2 we review some well-known results regarding the weak dispersion limit of the NLS equation. In section 3 we discuss the behavior of solutions corresponding to “single-jump” initial conditions, which are the starting point for our investigation. Then, in sections 4 and 5 we present the analytical calculations which are the main results of this work. In section 6 we demonstrate these results through numerical simulations of the NLS equation and obtain further information about the solution behavior, and in section 7 we discuss the application of our results to the generation of intense, ultra-short optical pulses. Appendix A.1 describes

our nondimensionalizations and our choice of units, Appendices A.2 and A.3 review some known results regarding genus-one (i.e., periodic) solutions of the NLS equation, the Whitham averaging method and the NLS-Whitham equations, and Appendix A.4 gives the details of some calculations whose results are presented in sections 3 and 4.

1 The NLS equation with small dispersion

In this section we recall some basic results regarding the behavior of solutions of the nonlinear Schrödinger (NLS) equation with small dispersion. This will establish the background and the notation necessary to extend these results in the following sections.

The semiclassical limit of the NLS equation. We start from the defocusing NLS equation (that is, the NLS in the normal dispersion regime in optical fibers) in dimensionless form:

$$i\varepsilon \frac{\partial q}{\partial t} - \frac{1}{2}\varepsilon^2 \frac{\partial^2 q}{\partial x^2} + |q|^2 q = 0, \quad (1.1)$$

where we assume $0 < \varepsilon \ll 1$. In the context of optical fibers, t represents the dimensionless propagation distance and x is the dimensionless retarded time (cf. Appendix A.1). To study the weak dispersion limit of the NLS Eq. (1.1), we first express the field $q(x, t)$ in a WKB form as

$$q(x, t) = \sqrt{\rho(x, t)} \exp[i\varphi(x, t)/\varepsilon], \quad (1.2)$$

where $\rho(x, t) = |q(x, t)|^2$ and $\varphi(x, t) = \varepsilon \arg q(x, t) = (\varepsilon/2) \ln[q^*(x, t)/q(x, t)]$ represent respectively the local intensity and the normalized local phase of $q(x, t)$. We then introduce the normalized phase gradient

$$u(x, t) = \partial\varphi(x, t)/\partial x, \quad (1.3)$$

that is, $u(x, t) = (i\varepsilon/2) (q_x^*(x, t)q(x, t) - q^*(x, t)q_x(x, t))/|q(x, t)|^2$. Throughout this work we refer to x and t as the space and time variables, respectively. By analogy with the fiber optics context, however, we will refer to $u(x, t)$ as the local *frequency* of the solution. With this decomposition, the NLS Eq. (1.1) can be written in the form of a conservation law:

$$\frac{\partial \rho}{\partial t} = \frac{\partial(\rho u)}{\partial x}, \quad (1.4a)$$

$$\frac{\partial(\rho u)}{\partial t} = \frac{\partial}{\partial x} \left(\rho u^2 + \frac{1}{2}\rho^2 - \frac{1}{4}\varepsilon^2 \rho \frac{\partial^2}{\partial x^2} \ln \rho \right). \quad (1.4b)$$

The weak dispersion limit of the defocusing NLS equation is defined as the problem of studying the solutions of Eq. (1.1) as $\varepsilon \rightarrow 0^+$ with initial condition expressed in terms of Eq. (1.2). The limit is singular, and it should be considered in the weak sense.

There are two main situations where the weak dispersion limit of the NLS equation is relevant: nonlinear fiber optics and Bose-Einstein Condensation (BEC). In the context of nonlinear fiber optics, the weak dispersion limit is relevant for the long-distance transmission of non-return-to-zero (NRZ) pulses, as discussed in Ref. [25], or for the generation of intense short optical pulses, as proposed in this work. In the context of BEC, the semiclassical limit applies due to the very small value of Planck's constant \hbar relative

to quantities associated with macroscopic objects, i.e., $\hbar = \epsilon$. Normalizations appropriate for long distance optical fiber communications were discussed in Ref. [14], whereas in appendix A.1, we discuss scalings and nondimensionalizations relevant for the generation of intense short optical pulses. We emphasize however that the results presented in this work apply equally well to Bose-Einstein condensates and to other physical context where the NLS equation is relevant, such as for example ferromagnetics and water waves.

Hydrodynamic analogy and dam-breaking problem. If both ρ and u are smooth and $\rho > 0$, and if $\epsilon \ll 1$, Eqs. (1.4) are approximated to leading order by the following reduced hydrodynamical system^[26, 34]

$$\frac{\partial}{\partial t} \begin{pmatrix} \rho \\ u \end{pmatrix} = \begin{pmatrix} u & \rho \\ 1 & u \end{pmatrix} \frac{\partial}{\partial x} \begin{pmatrix} \rho \\ u \end{pmatrix}. \quad (1.5)$$

Equation (1.5) is called the dispersionless NLS equation, and is used to describe a surface wave motion in shallow water. In the hydrodynamical setting, ρ and $-u$ represent respectively the depth and velocity of water, and x and t are dimensionless space and time. For $\rho > 0$, the eigenvalues $u \pm \sqrt{\rho}$ of the coefficient matrix are real, and the system (1.5) is strictly hyperbolic. This system, which is known as the shallow water wave equations and has been intensively studied (see e.g. Ref. [34]), can be rewritten in Riemann invariant (i.e., diagonal) form

$$\frac{\partial r_k}{\partial t} = s_k \frac{\partial r_k}{\partial x}, \quad k = 1, 2, \quad (1.6)$$

where the Riemann invariants $r_{1,2}(x, t)$ are given by

$$r_1 = u - 2\sqrt{\rho}, \quad r_2 = u + 2\sqrt{\rho}, \quad (1.7)$$

and the characteristic speeds $s_{1,2}(x, t)$ are

$$s_1 = \frac{1}{4}(3r_1 + r_2) = u - \sqrt{\rho}, \quad s_2 = \frac{1}{4}(r_1 + 3r_2) = u + \sqrt{\rho}.$$

Note that $s_k > 0$ implies a left-moving wave (i.e., $dx/dt = -s_k$), and that Eqs. (1.7) are equivalent to

$$\rho = \frac{1}{16}(r_2 - r_1)^2, \quad u = \frac{1}{2}(r_1 + r_2). \quad (1.8)$$

Since the system of PDEs described by Eq. (1.6) is strictly hyperbolic, it is possible to show that, for “rarefaction” initial data, namely, when $r_{1,2}(x, 0)$ are both monotonically decreasing functions of x , a global solution exists for all $t > 0$. In many cases of interest, however, the initial data do not satisfy this property and as a consequence they develop a shock, as we shall see in the following.

Square-wave initial conditions. Consider first the initial datum given by the following rectangular pulse of width $2L$:

$$\rho(x, 0) = \begin{cases} q_0^2 & |x| < L \\ 0 & |x| > L, \end{cases} \quad (1.9a)$$

$$u(x, 0) = 0, \quad (1.9b)$$

with $q_0 > 0$, corresponding in the optics framework to an NRZ pulse. The system of equations (1.5) with initial conditions (1.9) is known in the literature as the “dam-breaking” problem. (In the hydrodynamic analogy, the problem describes the behavior of a mass of water which is initially confined in a uniform,

spatially localized state by two dams located at $x = \pm L$ and both of which are removed at $t = 0$.) The Riemann invariants for this situation are shown as the dashed lines in Fig. 2.1a. Note that the initial data for the Riemann invariants r_1, r_2 corresponding to the initial condition (1.9) is not of rarefaction type. It is possible however to obtain initial data of rarefaction-type by properly redefining the initial value of the invariants r_1 and r_2 for $|x| > L$, as shown in Fig. 2.1b later. (This procedure is a special case of the process known as *regularization*, see next section.) Then the system has the following solution up to the time $t_0 = L/q_0$: for $0 < x < L + 2q_0 t$, it is

$$\rho(x, t) = \min\left\{q_0^2, \frac{1}{9}[2q_0 - (x - L)/t]^2\right\}, \quad (1.10a)$$

$$u(x, t) = \min\left\{0, -\frac{2}{3}[q_0 + (x - L)/t]\right\}, \quad (1.10b)$$

while for $x > L + 2q_0 t$, $\rho(x, t) = u(x, t) = 0$, with $\rho(-x, t) = \rho(x, t)$ and $u(-x, t) = -u(x, t)$ (cf. Ref. [25]). The full solution of the NLS equation (1.1) with initial condition (1.9), as obtained from numerical simulations (described in section 6) is depicted in Fig. 1.1a. (This kind of solution is usually called a *fan* in the context of hydrodynamics.) The speeds of the boundaries of the top ($\rho(x, t) = q_0^2$) and bottom ($\rho(x, t) = 0$) regions are easily obtained from Eqs. (1.10) (see also Fig. 2.1b later); these two speeds are respectively $s_2^- = q_0$ and $s_2^+ = -2q_0$.

Equations (1.10) cease to be valid beyond the time $t_0 = L/q_0$ when the boundaries of the top region meet at $x = 0$ (i.e., the time at which the left-moving characteristic emanating from $x = L$ meets with the right-moving characteristic from $x = -L$). An analytical expression for $q(x, t)$ when $t > L/q_0$ however can be obtained using the dispersionless limit of the scattering transform for the NLS equation^[31]. The corresponding behavior of the full solution of the NLS equation is shown in Fig. 1.1b. The appearance of small oscillations in the numerical solution in Figs. 1.1a,b was discussed in Ref. [14], and is the consequence of approximating the discontinuous initial data (1.9) with a continuous initial datum in the numerical simulations (as described in section 6). It should also be noted that some care must be taken regarding the regularization of the discontinuous initial datum (1.9) for Eq. (1.5), since a weak solution with a discontinuity is not unique. In fact, one can construct a different solution of (1.4) with a discontinuity. In our case, however, the regularization described in section 2 enforces the continuity of $\rho(x, t)$, thus removing the ambiguity and producing a unique solution.

Frequency jumps and high-frequency oscillations. In terms of optical pulses, the above results imply that the initial condition in Eq. (1.9) rapidly spreads out, as shown in Figs. 1.1a,b. This behavior can be partly prevented (or, alternatively, reinforced) by employing initial conditions with nontrivial phase. For example, consider the following:

$$u(x, 0) = \begin{cases} -u_0 & x < 0, \\ u_0 & x > 0, \end{cases} \quad (1.9b')$$

with $\rho(x, 0)$ still given by Eq. (1.9a). Hereafter, we will use $r_1^0(x)$ and $r_2^0(x)$ to refer to the value of the Riemann invariants (1.7) at $t = 0$. If $\rho(x, 0)$ is given by Eq. (1.9a) and $u(x, 0)$ by Eq. (1.9b'), for $|x| < L$ we have

$$r_1^0(x) = \begin{cases} -u_0 - 2q_0 & x < 0, \\ u_0 - 2q_0 & x > 0, \end{cases} \quad (1.11a)$$

$$r_2^0(x) = \begin{cases} -u_0 + 2q_0 & x < 0, \\ u_0 + 2q_0 & x > 0, \end{cases} \quad (1.11b)$$

as shown by dashed lines in Figs. 3.2a,b. Note that the value of the invariants can be redefined for $|x| > L$, since $\rho(x, 0) = 0$ there.

In terms of optical pulses, Eq. (1.9b') amounts to imposing a *frequency jump* at the center of the pulse ($x = 0$). If $u_0 > 0$, the right half of the pulse acquires a positive frequency and the left half a negative frequency. Thus, owing to the normal dispersion, the two halves of the pulse will tend to move towards each other.^[26] In terms of the hydrodynamical problem, this corresponds to assigning an inward initial velocity to the mass of water, as if two pistons were acting on each side of it. (For this reason, this case is often referred to as the “piston” problem.) Note that if $u_0 > 0$ the initial data $r_{1,2}^0(x)$ are increasing. Thus, another consequence of the initial frequency jump is that if $u_0 > 0$ a shock develops at $x = 0$, and the solution develops high-frequency oscillations, as shown in Fig. 3.1a. (This type of shock is called *collisionless*, or dispersive, to distinguish it from the usual type of shock, which is dissipative; e.g., see Ref. [34].) The characteristic frequency of these oscillations is $O(1/\epsilon)$ (i.e., one period of the oscillation shown in Fig. 3.1a is of order ϵ). If $u_0 < 0$ instead, the two halves of the pulse will move away from each other, and no shocks develop in this case. (In hydrodynamics, solutions such as this one are called of rarefaction type.) When the solution develops a shock, the hyperbolic system (1.5) ceases to be valid, and the solution of the NLS equation in the weak dispersion limit must be obtained by properly regularizing the hyperbolic system, as we briefly discuss next.

2 Regularization and the NLS-Whitham equations

The semiclassical limit of the NLS equation has been extensively studied in the last fifteen years; e.g., see Refs. [13, 22, 23, 24, 25, 27, 29, 31] for different approaches, the connection with the integrable character

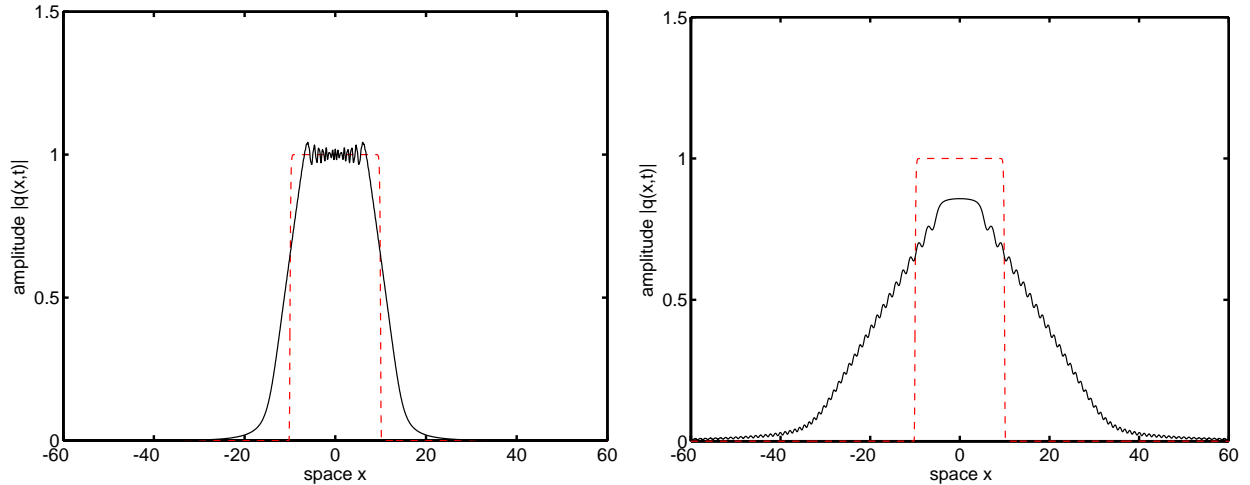


Figure 1.1: Deformation of an NRZ pulse (ie., the “dam-breaking” problem) defined by the initial conditions in Eqs. (1.9), with $q_0 = 1$, $L = 20$ and $\epsilon^2 = 0.1$: (a, left) $t' = 10$; (b, right) $t' = 40$, where $t' = t/\epsilon$. The critical time here is $t_0 = L/q_0 = 20$; hence Fig. 1.1a and Fig. 1.1b show the solution respectively before and after the time t_0 . The dotted lines show the initial condition, while the solid lines show the result of numerical simulations of the NLS equation (1.1), which are performed in terms of the fast time scale t' , as discussed in section 6.

and the multi-phase solutions of the NLS equation and with Whitham's averaging method. A self-contained description of the regularization process can be found in Ref. [25], together with a detailed treatment of the situation in which the initial condition contains only one frequency jump. Here we will limit ourselves to presenting a brief general overview and recalling some results which are relevant for the remainder of this work. Some additional details (which are necessary to perform the calculations described in sections 3 and 4) are contained in Appendices A.2 and A.3.

As we will see throughout this work, for certain kinds of initial conditions the solution of the NLS equation (1.1) with small dispersion develops high-frequency oscillations. When this happens, the approximate hyperbolic system (1.5) is inadequate to describe the dynamics of the solution, because of strong dispersive effects appearing due to the presence of high-frequency oscillations. An effective way to describe the behavior of the solution of the NLS equation in these situations is obtained by taking an average over these high-frequency oscillation via the Whitham technique, which consists in locally approximating the the solution by finite genus solutions of the NLS equation, then describing the global behavior as a slow modulation of this local periodic or quasi-periodic structure. The evolution of these modulations is then governed by the Whitham equations, which are obtained by averaging the conservation laws of the NLS equation over one period of the fast oscillations, and which express the local average of the quasi-periodic solutions with respect to these fast oscillations (cf. Refs. [12, 33, 34] for the Korteweg-de Vries equation).

Recall that the hyperbolic system (1.6) is a dispersionless limit of the NLS equation. The presence of high-frequency oscillations in the solution of NLS corresponds to the formation of a shock singularity in Eq. (1.6) generating strong dispersion, and the Whitham averaging technique then provides an appropriate dispersive regularization of this singularity. This regularization turns out to consist in enlarging the system (1.6) to include more than two Riemann invariants (as given by Eqs. (2.3) below) in such a way that the initial data for the enlarged system becomes of rarefaction type, which in turn implies that the system possesses a global solution for all values of time. The solution of the original problem is then described in terms of the solution of an NLS-Whitham equation of finite genus. The dispersionless equation (1.6) corresponds to the genus-zero NLS-Whitham equation. The value of the genus is determined by the specifics of the initial condition considered, since these determine the number of Riemann invariants which are needed to regularize the hyperbolic system.

Let us briefly review some features of the regularization and introduce the NLS-Whitham equations (see Appendices A.2 and A.3 and Refs. [13, 22, 25, 27] for more details). It is well-known that the NLS equation is integrable via the inverse scattering transform. The scattering problem associated with the defocusing NLS equation (1.1) is given by the eigenvalue problem^[2, 35] $\mathcal{L}\mathbf{v} = z\mathbf{v}$, where \mathbf{v} is a two-component vector, $z \in \mathbb{C}$ is the spectral parameter of the scattering problem, and where the Lax operator \mathcal{L} is defined by

$$\mathcal{L}\mathbf{v} = \begin{pmatrix} -i\varepsilon\partial_x & iq \\ -iq^* & i\varepsilon\partial_x \end{pmatrix} \mathbf{v}. \quad (2.1)$$

A genus- g solution of the NLS equation is associated to a genus- g hyperelliptic Riemann surface $R : w^2 = \mu_g(z)$, with

$$\mu_g(z) = \prod_{k=1}^{2g+2} (z - r_k). \quad (2.2)$$

The solution of the NLS equation (1.1) corresponding to Eq. (2.2) is described in terms of a Baker-Akhiezer function constructed from Riemann theta functions with g phases (e.g., see Ref. [5, 16] for details). The branch points r_1, \dots, r_{2g+2} of R determine the spectrum of \mathcal{L} . Since the Lax operator \mathcal{L} is self-adjoint, these

branch points are all real, and we label them so that $r_1 < r_2 < \dots < r_{2g+2}$. The spectrum of \mathcal{L} is then given by $(-\infty, r_1] \cup [r_2, r_3] \cup \dots \cup [r_{2g}, r_{2g+1}] \cup [r_{2g+2}, \infty)$.

For an exact genus- g solution of the NLS equation, the branch points r_1, \dots, r_{2g+2} are obviously constant, independent of space and time, owing to the isospectrality of the inverse scattering transform of the NLS equation. The solution then gives a quasi-periodic solution with g phases of the NLS equation, and with a small dispersion of order ε^2 implies that each period of the phase is of order ε (i.e., high-frequency oscillations of order $1/\varepsilon$).

Suppose now that the g -phase solution is slowly modulated. Then the spectral parameters r_k are expected to shift slightly (and even additional small gaps are expected to open in general). The shifted parameters are constant as the eigenvalues of the Lax operator \mathcal{L} . We can treat the modulation problem using a singular perturbation method as follows: if we consider modulations on the scale of (x, t) in the NLS equation (1.1), the modulations are of order one, and the oscillations are of order $1/\varepsilon$. This implies that one can treat the modulation problem as a small perturbation of the g -phase solution, which is the key of the Whitham averaging method. This method is based on an adiabatic assumption that the leading-order solution of the NLS equation (i.e., the g -phase solution) is preserved under the modulation, but with slowly changing parameters. Employing a standard averaging perturbation method, one introduces the fast and slow time and space scales respectively as $(x' = x/\varepsilon, t' = t/\varepsilon)$ and (x, t) . Then the first-order correction to the g -phase solution in the perturbation method compensates the motion of the parameters so that the parameters appear to be constant over regions of order one in (x, t) , but at the same time acquire small constant shifts due to the modulations in general. The corresponding equations for the spectral parameters with respect to the slow scales (x, t) are called the *NLS-Whitham equations*, or simply the Whitham equations, and are obtained by averaging the conservation laws of NLS with respect to the fast oscillations at order ε (see Appendix A.3 for more details).

It was shown in Refs. [13, 27] that the genus- g Whitham equations for the NLS equation can be written in the Riemann invariants form, in which the spectral parameters r_k give the Riemann invariants,

$$\frac{\partial r_k}{\partial t} = s_k(r_1, \dots, r_{2g+2}) \frac{\partial r_k}{\partial x}, \quad (2.3)$$

for $k = 1, \dots, 2g+2$. It then follows that for each $\varepsilon \neq 0$ the solution of the NLS-Whitham equations describes the slow modulation of finite-genus solutions of the NLS equation. It was also shown (cf. Lemma 4.1 in Ref. [25]) the following, which is the most important property of the NLS-Whitham equations:

Proposition 2.1 *The characteristic velocities s_k possess a double sorting property, i.e., $\forall k, l = 1, \dots, 2g+2$ they satisfy the two conditions*

$$\frac{\partial s_k}{\partial r_k} > 0, \quad (2.4a)$$

$$r_k < r_l \implies s_k < s_l, \quad (2.4b)$$

Then, as a consequence of 2.1, we have (Corollary 4.2 in Ref. [25]):

Corollary 2.2 *If the initial values of the r_k are each nonincreasing and if they satisfy the separability condition*

$$\max_{x \in \mathbb{R}} r_k^0(x) < \min_{x \in \mathbb{R}} r_{k+1}^0(x) \quad (2.5)$$

$\forall k = 1, \dots, 2g + 1$ at $t = 0$, the initial data is of rarefaction type, and therefore the hyperbolic system of equations (2.3) has a global solution for $t > 0$, i.e., it is regular.

In general, the initial conditions for the two Riemann invariants obtained from the dispersionless system (1.4) do not satisfy monotonicity and the separability condition (2.5). In other words, Eqs. (1.7) (that is, the system (2.3) with $g = 0$) in general do not have a global solution. The regularization process then consists in enlarging the set of Riemann invariants so that the resulting NLS-Whitham equations have a global solution. This is done by representing the initial data for the NLS Eq. (1.1) in such a way that all the Riemann invariants r_1, \dots, r_{2g+2} are monotonically decreasing functions of x at $t = 0$. Note that it is always possible to do so for piecewise-constant initial data, since in this case there is some ambiguity in how the spectrum of the Lax operator is represented in terms of the Riemann invariants. This ambiguity can then be exploited to redefine the initial datum for the Whitham Eqs. (2.3) by adding degenerate gaps (e.g., see Figs. 3.2 and 4.1). All of the solutions discussed in sections 3, 4 and 5 fall within the framework of piecewise-constant initial conditions. In this case the data at $t = 0$ are always genus-0, but highly degenerate, in the sense that they can be described in terms of a higher genus with degenerate gaps.

It should be noted that the adiabatic approximation (the use of the Whitham equations for the slow evolution) implies that the local genus of the solution is preserved. A separate issue is how the genus of the solution changes from one region to the next. This is a bifurcation problem through a critical point, and can be approached by regularization, i.e., by trying to patch two Whitham systems with different genus at this point. Our regularization acts as a “globalization”, in the sense that the Whitham equations with a proper (in general larger) genus now describes a global behavior beyond the perturbation range. For fixed x , a regular scheme must solve a connection problem in t because of the change of genus, and for fixed t one also needs to solve a connection problem to match regions with different genus.

It is also important to realize that for piecewise-constant initial data there is more than one way to

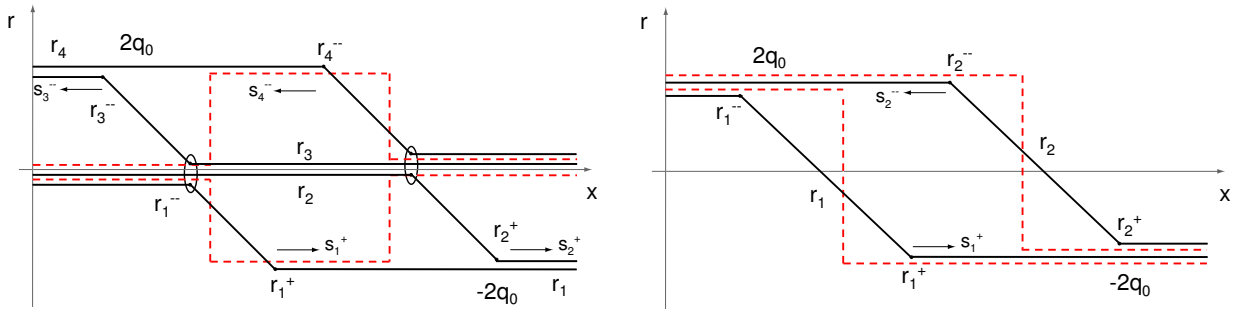


Figure 2.1: Evolution of the Riemann invariants in two equivalent cases. Dashed lines: the Riemann invariants at $t = 0$; solid lines: the invariants at $t \neq 0$. Figure 2.1a (left) corresponds to the square-wave initial datum in Eqs. (1.9) and Fig. 1.1, regularized by genus-1 data; Figure 2.1b (right) shows an equivalent diagram of the left one, and it is given by genus-0 data. Hereafter, the subscripts “-” and “+” refer to the value of the invariants respectively to the left and to the right of their initial discontinuity. The ellipses in Fig. 2.1a indicate “locking” points, i.e., points x_* for which $r_1(x_*, t) = r_2(x_*, t) = r_3(x_*, t)$ (on the left) and $r_2(x_*, t) = r_3(x_*, t) = r_4(x_*, t)$ (on the right) for all t . This implies that the regularization at those points is trivial. Finally, note that the initial conditions $r_{1,2}^0(x)$ in the equivalent figure (Fig. 2.1b) have been redefined whenever $p(x, 0) = 0$ (i.e., $u(x)$ itself is not defined in the NLS-Whitham equation when $p(x) = 0$, see Eqs. (A.9)).

regularize the initial datum (e.g., see Figs. 2.1a,b). The minimum number of Riemann invariants that are necessary so that the system becomes regular is related to the genus of the solution of the NLS-Whitham equations. That is, $2g + 2$ invariants correspond to a genus- g solution of Eqs. (2.3). The local genus of the solution of the NLS equation is roughly speaking the number of distinct frequencies which are locally present in the solution over regions of order one in (x, t) . Since the Riemann invariants are the branch points of the spectrum of the finite-genus solution of NLS which locally approximates the full solution, it is then clear that the local genus is equal to the number of gaps determined by the local value of the Riemann invariants (e.g., see Figs. 5.1 and 5.2). The opening or closing of one of the gaps for some values of (x, t) corresponds to a local change of genus in the solution of the NLS equation. Note however that all finite-genus solutions of the NLS equation with non-zero genus become singular in the limit $\varepsilon \rightarrow 0^+$. In this sense, the solution of the Whitham equations represents a weak limit, since when $g \neq 0$ the solutions of the NLS equation only converge in an average sense (i.e., weak convergence).

Finally, with regards to Fig. 2.1 we should note that genus-1 data is necessary in order to preserve the value of $u(x, 0)$. With step initial data, however, no gap opens during propagation, which means that the data is degenerate, producing a genus-0 solution. The situation would be different in the case of non-step initial data (e.g., if the transition from $\rho(x, 0) = 0$ to $\rho(x, 0) = q_0^2$ were continuous); in that case oscillations would appear, as described in Ref. [14].

3 Single-jump initial conditions

We now briefly summarize some results from Ref. [25] relative to a single-jump initial datum, since they provide the basis for the framework that will be used to analyze the more complicated scenarios discussed in the remainder of this work. We will consider the constant-amplitude wave given by the (single-jump) initial condition in Eqs. (1.9a) and (1.9b'), where we take $L \rightarrow \infty$. The value of the original Riemann invariants in the genus-0 system Eq. (1.6) at $t = 0$ is again given by Eqs. (1.11), which are now valid $\forall x \in \mathbb{R}$. Four different situations arise depending on the size of the frequency jump $2u_0$, as shown in Figs. 3.1a–d:

- (i) $u_0 > 2q_0 > 0$ (Lemma 4.3 and Theorem 4.4 in Ref. [25]).

Since $u_0 > 0$, the original Riemann invariants $r_{1,2}^0(x)$ are increasing functions of x , and therefore the genus-0 system (1.6) does not have a global solution. In this case the problem is regularized by considering the genus-1 NLS-Whitham equations. (That is, four invariants are necessary so that the resulting system has a global solution.) The Riemann invariants are related to the solution at $t = 0$ as follows:

$$\begin{aligned} r_1 &= -u_0 - 2q_0 & \forall x, & & r_3 &= u_0 \pm 2q_0 & \text{for } x \gtrless 0, \\ r_2 &= -u_0 \pm 2q_0 & \text{for } x \lesseqgtr 0, & & r_4 &= u_0 + 2q_0 & \forall x, \end{aligned}$$

with the upper/lower signs corresponding to the upper/lower inequality for x , respectively. The qualitative evolution of these Riemann invariants is shown in Fig. 3.2a. The solution develops a region of genus-1 high-frequency oscillations in the central portion of the pulse, surrounded by a genus-0 region, as illustrated in Fig. 3.1a and Fig. 3.3a. As shown in Fig. 3.1a, the genus-1 portion of the solution describes slow modulations of high-frequency oscillations, as would be the case in a wave packet. The genus-1 portion of the solution is located in the region $|x| < s_3^- t$. The characteristic velocities are

$s_3^- = -s_2^+, s_3^+ = -s_2^-$, with $s_3^- > s_3^+ > 0$ and

$$s_3^- = (u_0 + q_0) \left[1 + u_0 q_0 / (u_0 + q_0)^2 \right], \quad s_3^+ = u_0 \left[1 - 3a(1-a)K_1 - 2a^2 K_2 \right] / (1 - aK_1) \quad (3.1)$$

(cf. Eqs. (4.16) and (4.17) in Ref. [25]), where $a = 2q_0/u_0 < 1$ and

$$1 - K_n = \int_0^{\pi/2} \frac{\sin^{2n+2} \theta}{\sqrt{(1 + a \sin^2 \theta)(1 + a \cos^2 \theta)}} d\theta \bigg/ \int_0^{\pi/2} \frac{\sin^2 \theta}{\sqrt{(1 + a^2 \sin^2 \theta)(1 + a^2 \cos^2 \theta)}} d\theta.$$

Hereafter, the superscripts “−” and “+” refer to the value of the Riemann invariants respectively to the left and to the right of the discontinuities at $t = 0$ (cf. Fig. 3.2). Note that, owing to Eq. (2.3), positive values of s correspond to left-moving Riemann invariants, and that for regularized, non-increasing invariants $r^-(x) \geq r^+(x) \forall x \in \mathbb{R}$.

(ii) $0 < u_0 < 2q_0$ (Lemma 4.5 and Theorem 4.6 in Ref. [25]).

Again, since $u_0 > 0$, the genus-0 Whitham equations do not have a global solution. This case is regularized by the genus-2 NLS-Whitham equations. The six Riemann invariants are related to the solution at $t = 0$ as follows:

$$\begin{aligned} r_1 &= -u_0 - 2q_0 \quad \forall x, & r_4 &= -u_0 + 2q_0 \quad \forall x, \\ r_2 &= \pm u_0 - 2q_0 \quad \text{for } x \lesseqgtr 0, & r_5 &= \pm u_0 + 2q_0 \quad \text{for } x \lesseqgtr 0, \\ r_3 &= u_0 - 2q_0 \quad \forall x, & r_6 &= u_0 + 2q_0 \quad \forall x. \end{aligned}$$

The qualitative evolution of these Riemann invariants is shown in Fig. 3.2b. Even though $g = 2$ is necessary to regularize the initial data, no genus-2 region appears. The solution develops a genus-0 flat region (a degenerate genus-2 region) in the central portion of the pulse, surrounded by genus-1 high-frequency oscillations, as illustrated in Fig. 3.1b. The genus-0 and genus-1 portions of the solution are respectively located in the regions $|x| < s_5^+ t$ and $s_5^+ t < |x| < s_5^- t$, with $s_5^+ = -s_2^-$, $s_5^- = -s_2^+$, and where $s_5^- > s_5^+ > 0$. The characteristic velocities are (Eqs. (4.28) in Ref. [25])

$$s_5^+ = q_0 - \frac{1}{2}u_0, \quad s_5^- = (u_0 + q_0) \left[1 + u_0 q_0 / (u_0 + q_0)^2 \right]. \quad (3.2)$$

Furthermore, in the genus-0 region, the solution takes the value $\rho = \frac{1}{16}(r_2^0 - r_1^0)^2$, i.e.,

$$\rho = q_0^2 \left[1 + u_0 / 2q_0 \right]^2. \quad (3.3)$$

Note that the amplitude of the genus-0 (non-oscillatory) region at the center increases with increasing modulation strength u_0 . At the same time, however, the dependence of s_5^+ on u_0 implies that the width of the genus-0 region decreases with increasing modulation strength, and the region ceases to exist when $u_0 > 2q_0$. The maximum possible amplitude that can be obtained in this way is thus $\rho_{\max} = 4q_0^2$, obtained for $u_0 = 2q_0$.

This case, $0 < u_0 < 2q_0$, is the most interesting case for applications because, unlike the high-frequency oscillations in the genus-1 portion, the high-amplitude genus-0 region can survive an appropriate filtering and produce short, high-intensity optical pulses. As mentioned above, however, the maximum amplitude that can be obtained with this arrangement is limited, i.e., $q = (1 + u_0/q_0)q_0 < 2q_0$. In the next section we will see how this limit on the maximum pulse amplitude can be overcome by employing more than one frequency jump.

(iii) $-2q_0 < u_0 < 0$ (Theorem 4.7 in Ref. [25]).

Since $u_0 < 0$, the Riemann invariants $r_{1,2}^0(x)$ are decreasing functions of x , and therefore the genus-0 NLS-Whitham equations (1.5) with the Riemann invariants defined as in Eq. (1.7) has a global solution, and no regularization is necessary. The solution develops a depression zone in the center, as illustrated in Fig. 3.1c. More precisely (Eqs. (4.31) and (4.33) in Ref. [25]),

$$\rho(x,t) = \begin{cases} q_0^2 [1 + u_0/(2q_0)]^2 & |x| < s_2^+ t, \\ [x + (u_0 + 2q_0)t]^2 / 9t^2 & s_2^+ t < |x| < s_2^- t, \\ q_0^2 & |x| > s_2^- t, \end{cases}$$

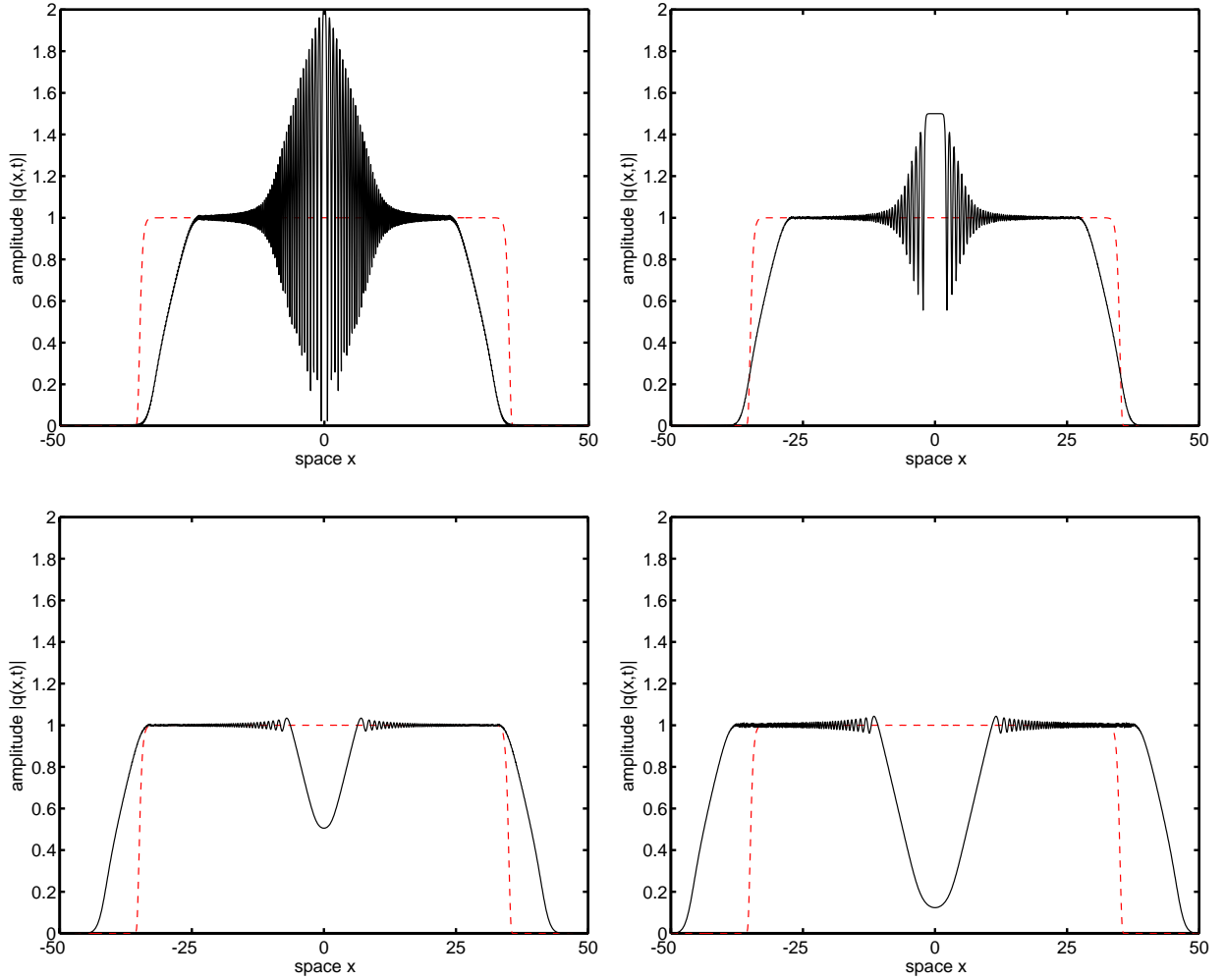


Figure 3.1: Deformation of an NRZ pulse in the presence of an initial frequency jump: (a, top left) $u_0 = 2.01$; (b, top right) $u_0 = 1$; (c, bottom left) $u_0 = -1$; (d, bottom right) $u_0 = -2.5$. The dotted line shows the initial condition; the solid line shows the result of numerical simulations of the NLS equation, performed as discussed in section 6. In all four cases it is $q_0 = 1$, $L = 35$, and $\epsilon^2 = 0.1$, and the solution is shown at $t' = 20$, where $t' = t/\epsilon$.

where

$$s_2^+ = \frac{1}{2}(u_0 + 2q_0), \quad s_2^- = q_0 - u_0. \quad (3.4)$$

(iv) $u_0 < -2q_0$ (Lemma 4.8 and Theorem 4.9 in Ref. [25]).

This case is regularized by the genus-1 NLS-Whitham equations (1.5). The Riemann invariants at

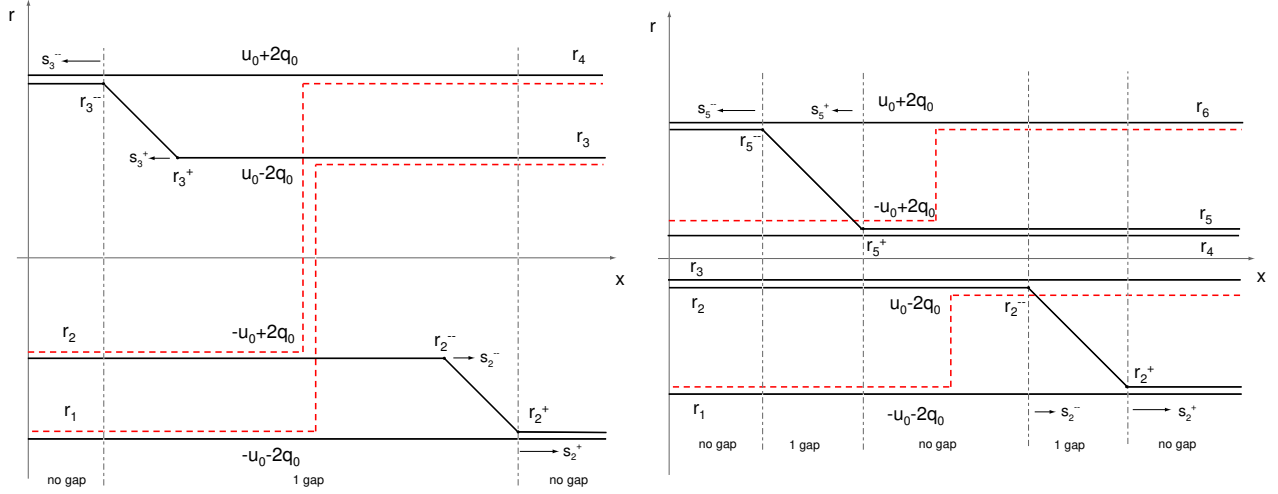


Figure 3.2: Qualitative diagrams illustrating the evolution of the Riemann invariants: (a, left) $u_0 > 2q_0$, with a single, expanding genus-1 region; (b, right) $0 < u_0 < 2q_0$, with an expanding genus-0 region surrounded by expanding genus-1 regions on either side. Dashed lines: the original invariants $r_{1,2}^0(x)$ at $t = 0$; solid lines: the regularized invariants at $t \neq 0$; dot-dashed vertical lines: boundaries between regions of different genus. Note that the connecting segments between r_2^\pm in Fig. 3.2a,b, r_3^\pm in Fig. 3.2a and r_5^\pm in Fig. 3.2b are actually curved, and are only represented here by straight lines for simplicity (e.g., see Ref. [7]).

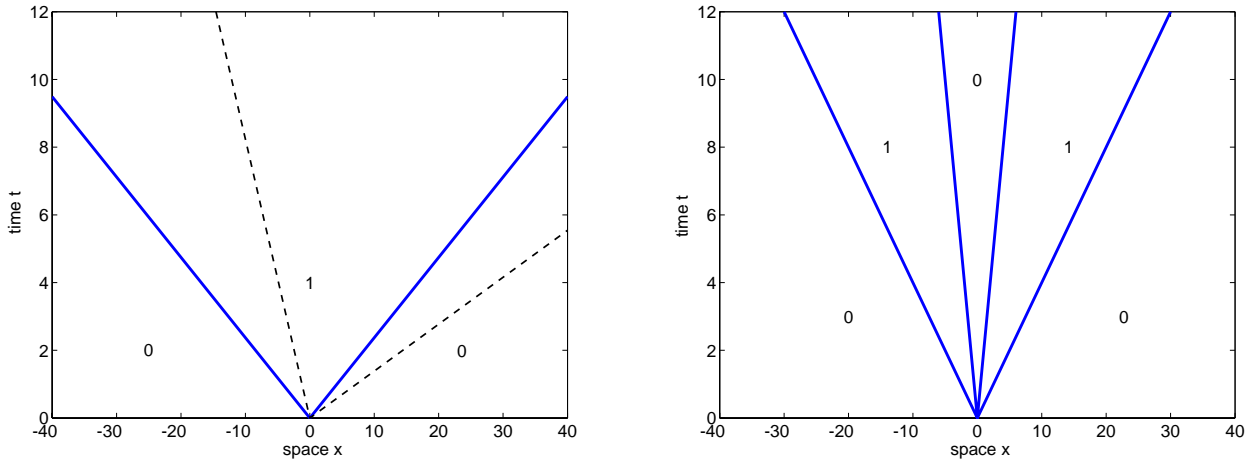


Figure 3.3: The boundaries between regions of genus-0 and genus-1 in the (x, t) -plane corresponding the cases shown in Fig. 3.2: (a, left) $u_0 = 5/2$, corresponding to case (i) and Figs. 3.1a and 3.2a; (b, right) $u_0 = 1$, corresponding to case (ii) and Figs. 3.1b and 3.2b. Dashed lines: the same boundaries after adding a constant frequency offset $u_{\text{avg}} = 3$ to both sides of the jump, as discussed in section 4.

$t = 0$ are defined by:

$$\begin{aligned} r_1 &= u_0 \pm 2q_0 \quad \text{for } x \lesssim 0, & r_3 &= -u_0 - 2q_0 \quad \forall x \\ r_2 &= u_0 + 2q_0 \quad \forall x, & r_4 &= -u_0 \pm 2q_0 \quad \text{for } x \gtrsim 0, \end{aligned}$$

The corresponding solution is shown in Fig. 3.1d. Even though $g = 1$ is necessary to regularize the initial data, the gap never opens, and this case produces a degenerate genus-0 solution. The solution is similar to the one in the previous case, except that $q(x, t)$ tends to zero at $x = 0$. More precisely, $\rho(x, t) = q_0^2$ for $|x| > s_4^- t$ and $\rho(x, t) = 0$ in the limit $\varepsilon \rightarrow 0^+$ in the region $|x| < s_4^+ t$, where (Eqs. (4.36) in Ref. [25])

$$s_4^+ = -u_0 - 2q_0, \quad s_4^- = -u_0 + 2q_0. \quad (3.5)$$

(The nonzero value of $q(0, t)$ in Fig. 3.1d is due to the finiteness of ε in the numerical simulations.) Furthermore, the solution does not develop genus-1 regions (the high-frequency oscillations visible in Fig. 3.1d disappear in the limit $\varepsilon \rightarrow 0^+$ in the case of step initial data).

The calculation of the characteristic speeds for the Riemann invariants is based on the formulation of the NLS-Whitham equations. We refer the reader to appendices A.3 and A.4 and to Refs. [6, 7, 25] for further details. Note that the outer boundaries of the genus-1 region are given by $x = \pm s_{\text{outer}} t$, where s_{outer} is the same in case (i) and case (ii): $s_{\text{outer}} = (u_0 + q_0) [1 + u_0 q_0 / (u_0 + q_0)^2]$ (cf. s_3^- in Eq. (3.1) and s_5^- in Eq. (3.2)). Note also that the location of the boundaries between regions of genus-0 and genus-1 in the numerical simulations shown in Figs. 3.1a–d agrees very well with the analytical results just presented, even though the value of ε used is not very small.

Case (ii) is the most interesting for applications because of the high-amplitude genus-0 region. Also, in cases (iii) and (iv) (i.e., when $u_0 < 0$) the solution is only of genus-0, but lower-amplitude. For this reason we will mainly focus our attention to the case of positive frequency jumps. Hereafter, we refer to case (ii) as a “sub-critical” frequency jump and to case (i) as a “super-critical” frequency jump. More precisely,

Definition 3.1 *We say that a single frequency jump located at $x = x_0$ is super-critical if $r_1^0(x_0^+) > r_2^0(x_0^-)$, sub-critical if $r_1^0(x_0^+) < r_2^0(x_0^-)$, where as usual $r_k^0(x^\pm) = \lim_{\Delta x \rightarrow 0^\pm} r_k^0(x + \Delta x)$.*

In the following sections we generalize the above solutions and discuss the behavior of solutions of the finite-genus NLS-Whitham equations in the presence of an arbitrary number of jumps in the initial data.

4 Behavior of finite-genus solutions: Two frequency jumps

More complicated situations than those described in the previous section arise when the initial conditions contain more than one frequency jump. The main purpose of this and the following section is to study the interaction among finite-genus solutions of the NLS-Whitham equations generated by those frequency jumps. First of all, however, let us briefly discuss the effect of adding a non-zero average frequency across the jump. The Galilean invariance of the NLS equation implies that it is possible to redefine the local frequency $u(x, 0)$ up to an arbitrary additive constant. The effect of such a constant, representing a global frequency translation, is just a change in the overall group velocity of the solution. More precisely, if $q_o(x, t)$ is a solution of Eq. (1.1), so is

$$q_c(x, t) = \exp[i(cx - c^2 t/2)/\varepsilon] q_o(x + ct, t), \quad (4.1)$$

for any constant c . Corresponding to Eq. (4.1) there exists a Galilean symmetry of the NLS-Whitham equations (2.3) for the Riemann invariants: namely, if $r_j(x, t)$ is a solution of the Whitham equations (2.3), then so is the translated solution $r_j(x + ct, t) + c$. Note from Eq. (4.1) that a positive frequency c/ε corresponds to a negative shift $-c$ in the group velocity dx/dt . Also, as an effect of the Galilean transformation (4.1) the rescaled frequency of the transformed solution is shifted by c , i.e., $u_c(x, t) = \varepsilon \partial_x [\arg q_c(x, t)] = c + \varepsilon \partial_x [\arg q_o(x + ct, t)]$. In terms of the decomposition of the (x, t) -plane into regions of different genus, we thus have the following:

Lemma 4.1 *The boundaries between genus-0 and genus-1 regions for a single frequency jump upon adding a nonzero average frequency u_{avg} to the initial condition are given by $x = s_{\pm}t$, where $s_{\pm} = \pm s_{\text{old}} + u_{\text{avg}}$, and where s_{old} is still given by Eqs. (3.1), (3.2), (3.4) and (3.5) in cases (i–iv), respectively.*

Thus, adding a nonzero frequency offset to both sides of a single frequency jump has the effect of tilting the corresponding boundaries between regions of different genus, as shown in Fig. 3.3a. If only one jump is present, it is obviously possible to choose the average frequency so that both of the boundaries of the outermost genus-0 region move in the same direction. In the presence of several frequency jumps, however, is not always possible to do so, as will be discussed later. Because of the Galilean invariance, we will sometimes describe the initial condition for $u(x, 0)$ in terms of the frequency jumps, defined as $C_j = u(X_j^+, 0) - u(X_j^-, 0)$ for all $j = 1, \dots, N$, where N is the total number of jumps and X_1, \dots, X_N are the jump locations.

We now turn to initial conditions with two frequency jumps. We will consider constant-amplitude initial conditions with $|q(x, 0)| = q_0 \forall x \in \mathbb{R}$. For simplicity we will take symmetric jumps of size $C_1 = C_2 =: 2u_0$ located at $X_2 = -X_1 = \Delta X/2 > 0$, so that $2u_0$ is the size of each frequency jump, as in the single-jump case. That is, let

$$u(x, 0) = \begin{cases} -2u_0 & x < -\Delta X/2, \\ 0 & |x| < \Delta X/2, \\ 2u_0 & x > \Delta X/2, \end{cases} \quad (4.2)$$

again with $|q(x, 0)| = q_0 > 0 \forall x \in \mathbb{R}$. In the absence of either one of the two jumps, the solution would behave according to the theory described in Section 3, with the only exception that the average frequency across the jump is now nonzero. More precisely, since the average frequency at $x = \pm \Delta X/2$ is $\pm u_0$, the solutions described in the previous section would move with velocity $\mp u_0$. In other words, the central portion of the solutions described in Section 3 will tend to move towards each other if $u_0 > 0$ and away from each other if $u_0 < 0$. As we will see, this description provides an accurate picture of the overall solution at sufficiently small propagation times. After this initial stage, however, significant interaction effects appear.

In analogy with the calculations described in Section 3, let us now proceed to analyzing the solution by looking at the Riemann invariants. The initial values $r_{1,2}^0(x)$ of the non-regularized Riemann invariants for the genus-0 NLS-Whitham equations (1.6) are

$$r_1^0(x) = \begin{cases} -2q_0 - 2u_0 & x < -\Delta X/2, \\ -2q_0 & |x| < \Delta X/2, \\ -2q_0 + 2u_0 & x > \Delta X/2, \end{cases} \quad r_2^0(x) = \begin{cases} 2q_0 - 2u_0 & x < -\Delta X/2, \\ 2q_0 & |x| < \Delta X/2, \\ 2q_0 + 2u_0 & x > \Delta X/2. \end{cases} \quad (4.3)$$

These invariants are shown as dashed lines in Figs. 4.1a–d. Since expressing the values of all the regularized Riemann invariants at $t = 0$ in terms of the initial datum would be rather tedious, and since all the values can be easily inferred from Figs. 4.1a–d, we omit the formulae for brevity.

Based on Proposition 2.1 and Corollary 2.2, the following four scenarios arise depending on the size of the frequency jumps:

(i) $u_0 > 2q_0 > 0$:

This case is regularized by the genus-2 NLS-Whitham equations (i.e., with six invariants), as illustrated in Fig. 4.1a, where the (two) original and (six) regularized Riemann invariants are shown respectively by dashed and solid lines.

The regions of genus-0, 1 and 2 for the solution of the NLS equation are shown in the bifurcation diagram in Fig. 4.2a. Both jumps are super-critical individually, so two genus-1 regions open up, one at the location of each frequency jump. These two regions interact and they create a genus-2 region at the center of the solution. The genus-2 region then expands forever (cf. Propositions 4.4 and 4.7). In terms of the numerical simulations described in the next section, this case corresponds to Fig. 6.1a.

(ii) $q_0 < u_0 < 2q_0$:

This case is regularized by the genus-4 NLS-Whitham equations (i.e., with ten invariants), as illustrated in Fig. 4.1c,d, where the original and regularized Riemann invariants are shown at two different values of t .

The regions of genus-0, 1 and 2 for the solution of the NLS equation are shown in the bifurcation diagram in Fig. 4.2b. Both jumps are sub-critical individually; so two genus-0 regions open up initially at the location of each frequency jump (each surrounded by genus-1 regions, as in case (ii) of section 3). As these two portions of the solution interact, a genus-0 region forms temporarily in the central portion of the solution. This region disappears after a while, however, and a genus-2 region forms which expands forever as in the previous case (cf. Propositions 4.4, 4.7 and 4.8). In terms of the numerical simulations, this case corresponds to Fig. 6.1b and Figs. 6.3c,d.

(iii) $0 < u_0 < q_0$:

This case is also regularized by the genus-4 NLS-Whitham equations. The original and regularized Riemann invariants are shown in Fig. 4.1b, and the regions of genus-0, 1 and 2 for the solution of the NLS equation are shown in the bifurcation diagram in Fig. 4.2d.

As in the previous case, the individual jumps are sub-critical, so two genus-0 regions open up initially at the location of each frequency jump. Also similarly to the previous case, a genus-0 region forms in the central portion of the solution as the two genus-0 portions of the solution interact. Contrary to the previous case, however, the genus-0 portion of the solution now persists and expands forever (cf. Propositions 4.4, 4.7 and 4.8). Numerical simulations corresponding to this case are shown in Fig. 6.1c and Figs. 6.3a,b.

(iv) $u_0 < 0$:

As in the single-jump case, two expanding depression regions form at the location of each frequency jump. Eventually, these regions merge to form a unique depression zone. As in the single-jump case, the details of the regularization process vary depending on the value of u_0 . Because the solution is always genus-0, however, this case is not as interesting as the previous ones in terms of applications, and therefore it will not be investigated further.

Let us now discuss more quantitatively the behavior of the solutions in each of the above scenarios. When $u_0 > 0$ as in cases (i)–(iii), the initial values of the non-regularized Riemann invariants $r_{1,2}^0(x)$ are increasing functions of x , and one has:

$$\max_{x \in \mathbb{R}} r_1^0(x) = r_1^0(\infty) = \lim_{x \rightarrow \infty} r_1^0(x) = 2(u_0 - q_0), \quad (4.4a)$$

$$\min_{x \in \mathbb{R}} r_2^0(x) = r_2^0(-\infty) = \lim_{x \rightarrow -\infty} r_2^0(x) = -2(u_0 - q_0). \quad (4.4b)$$

As we will see in section 6, cases (ii) and (iii) offer the most useful behavior for practical applications. In particular, the case $u_0 = q_0$, which is the separatrix between cases (ii) and (iii), is especially interesting

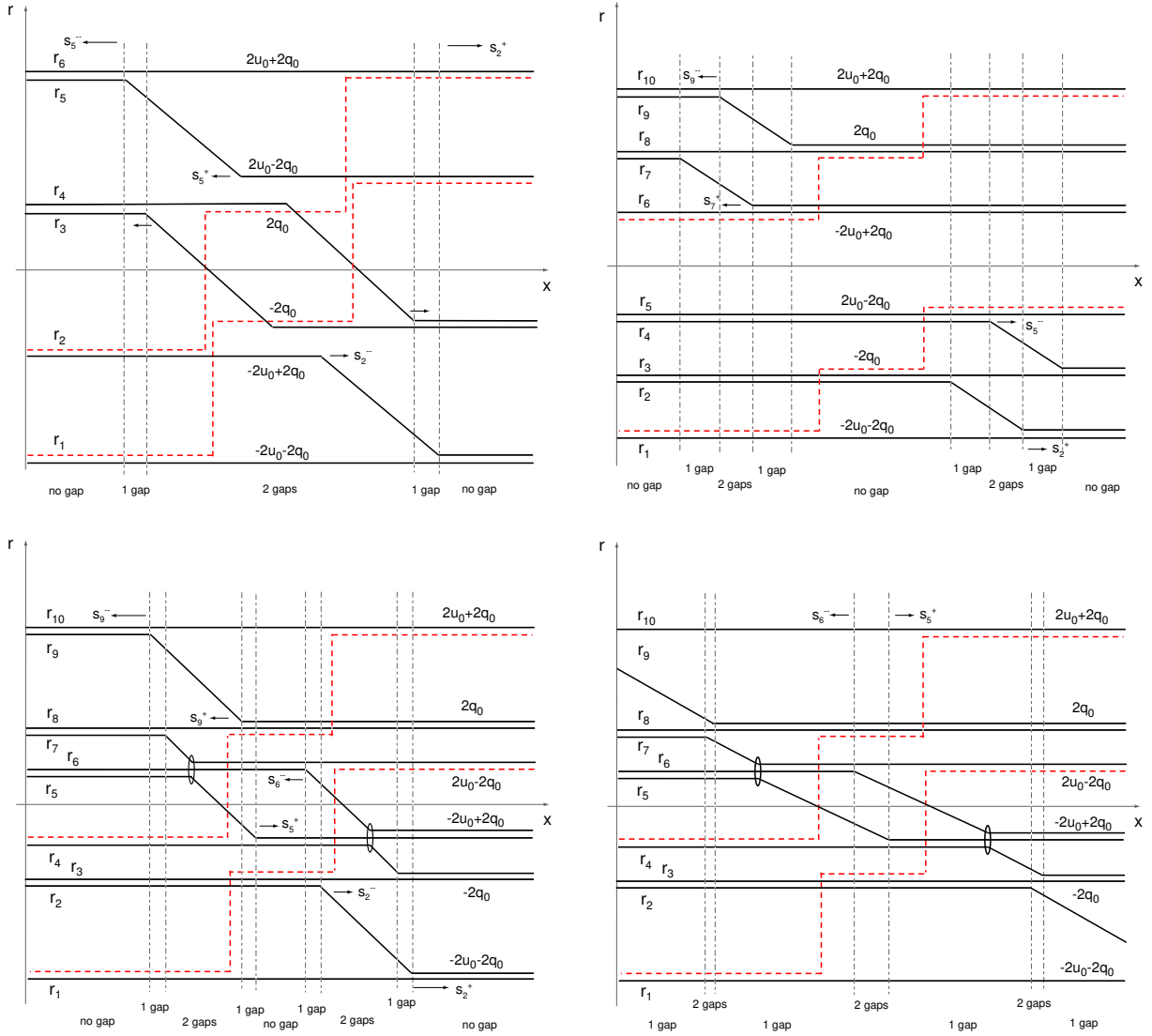


Figure 4.1: Qualitative diagrams illustrating the evolution of the Riemann invariants: (a, top left) $u_0 > 2q_0$, corresponding to case (i) and showing expanding genus-1 and genus-2 regions; (b, top right) $0 < u_0 < q_0$, corresponding to case (iii) and showing an expanding genus-0 central region; (c, bottom left) $q_0 < u_0 < 2q_0$ corresponding to the intermediate case (ii), and showing the invariants at small time t and a temporary genus-0 region in the center; (d, bottom right) the same intermediate case (i.e., $q_0 < u_0 < 2q_0$ as in (c)), but now showing the solution at large time t and an expanding genus-2 region in the center. Dashed lines: the original invariants $r_{1,2}^0(x)$ at $t = 0$; solid lines: the regularized invariants at $t \neq 0$; dot-dashed vertical lines: boundaries between regions of different genus. As in section 2, the ellipses in Figs. 4.1c,d indicate “locking points”, i.e., locations corresponding to the same value of $x \forall t$ (cf. Remark 4.5.5). Finally, note that, as in Fig. 3.2, those portions of the invariants that coincide in the limit $\varepsilon \rightarrow 0^+$ can be omitted when calculating the local genus.

since it produces a high-amplitude genus-0 region of constant width at the center of the pulse, as shown in Fig. 4.2c. This case is regularized by the genus-3 NLS-Whitham equations, corresponding to Fig. 4.1b with r_5 and r_6 deleted and where now $r_1^0(\infty) = r_2^0(-\infty)$, since $u_0 = q_0$. Hereafter, we will call the case $u_0 = q_0$ the “critical” two-jump case, and we will refer to cases (ii) and (iii) as the super-critical and sub-critical two-jump cases, respectively. More precisely,

Definition 4.2 *We say that an arbitrary collection of positive frequency jumps C_1, \dots, C_N located at positions X_1, \dots, X_N is collectively super-critical if $r_1^0(\infty) > r_2^0(-\infty)$, collectively sub-critical if $r_1^0(\infty) < r_2^0(-\infty)$, and collectively critical if $r_1^0(\infty) = r_2^0(-\infty)$, where as usual $r_k^0(\pm\infty) = \lim_{x \rightarrow \pm\infty} r_k^0(x)$.*

Note the difference between the above and Definition 3.1, which distinguishes whether a single jump is *individually* sub-critical or super-critical.

It should be noted that, even though the NLS-Whitham equations with $g = 3, 4$ are necessary to regularize the data in some cases, only the genus $g \leq 2$ appears in the solution with two frequency jumps (similarly to the scenario with a single frequency jump). Note also that, unlike the case when a single phase is present, calculating analytically the precise location of the boundaries between different multi-phase regions after the individual portions of the solutions have come into contact is a highly nontrivial task, and we have not attempted to do so. However, it is possible to calculate the velocity of all boundaries between genus-0 and genus-1 regions. The main reason for the difference between the two types of boundaries is that, upon removal of degenerate gaps, the calculation of characteristic speeds in regions of genus-1 is expressed in terms of elliptic integrals and the boundary with genus-0 turns out to be a straight line (see Lemma 4.3 below), whereas the characteristic speeds in regions of genus-2 require the evaluation of hyperelliptic integrals (e.g., see Ref. [17]).

The explicit calculation of a few characteristic speeds is reported in appendix A.4. Since such calculations are rather lengthy, however, and since the methods used are described in Refs. [6, 7, 25], here we omit the details relative to all the different cases, and we limit ourselves to summarizing the main results.

Lemma 4.3 *All boundaries between genus-0 and genus-1 regions are given by straight lines.*

Proof. The result follows from Eqs. (2.3) and by noting that the characteristic speeds are constant since all the invariants are constant in the genus-0 portion. \square

This result is obviously independent of the number of frequency jumps present, and is just a special case of a generic feature of hyperbolic systems: if one side of the initial condition is constant, there is a solution in terms of simple waves, for which the characteristics are straight lines^[34].

Proposition 4.4 *The boundaries between genus-0 and genus-1 regions before the interaction are given by straight lines with the same velocities as in Eq. (3.1) and Eqs. (3.2) upon application of the appropriate Galilean shifts. That is, $s_{i,\pm} = \pm s_i + u_0$ for the regions relative to the frequency jump to the left and $s_{i,\pm} = \pm s_i - u_0$ for those relative to the frequency jump to the right.*

Proof. The result follows by direct computation of the characteristic speeds in the NLS-Whitham equations (2.3), but is consistent with Lemma 4.1 regarding the application of a constant offset to a single frequency jump, showing that before interaction the behavior of the solution in each region is unaffected by the presence of the other jump. \square

Remark 4.5. In case (ii) (cf. Figs. 4.1c,d and Fig. 4.2b), it is $r_5(x_*,t) = r_6(x_*,t) = r_7(x_*,t)$ for all t , where $x_*(t) = \max\{x \in \mathbb{R} : r_5(x,t) = 2(u_0 - q_0)\}$. That is, the three invariants are “locked” together at that point. Similarly, if one defines $x_{**}(t) = \min\{x \in \mathbb{R} : r_6(x,t) = -2(u_0 - q_0)\}$, it is $r_4(x_{**},t) = r_5(x_{**},t) = r_6(x_{**},t)$ for all t . This locking phenomenon is identified by the two ellipses in Figs. 4.1c,d (see also Fig. 2.1a). Moreover, since two of the three invariants always coincide in a neighborhood of x_* or x_{**} , in each case

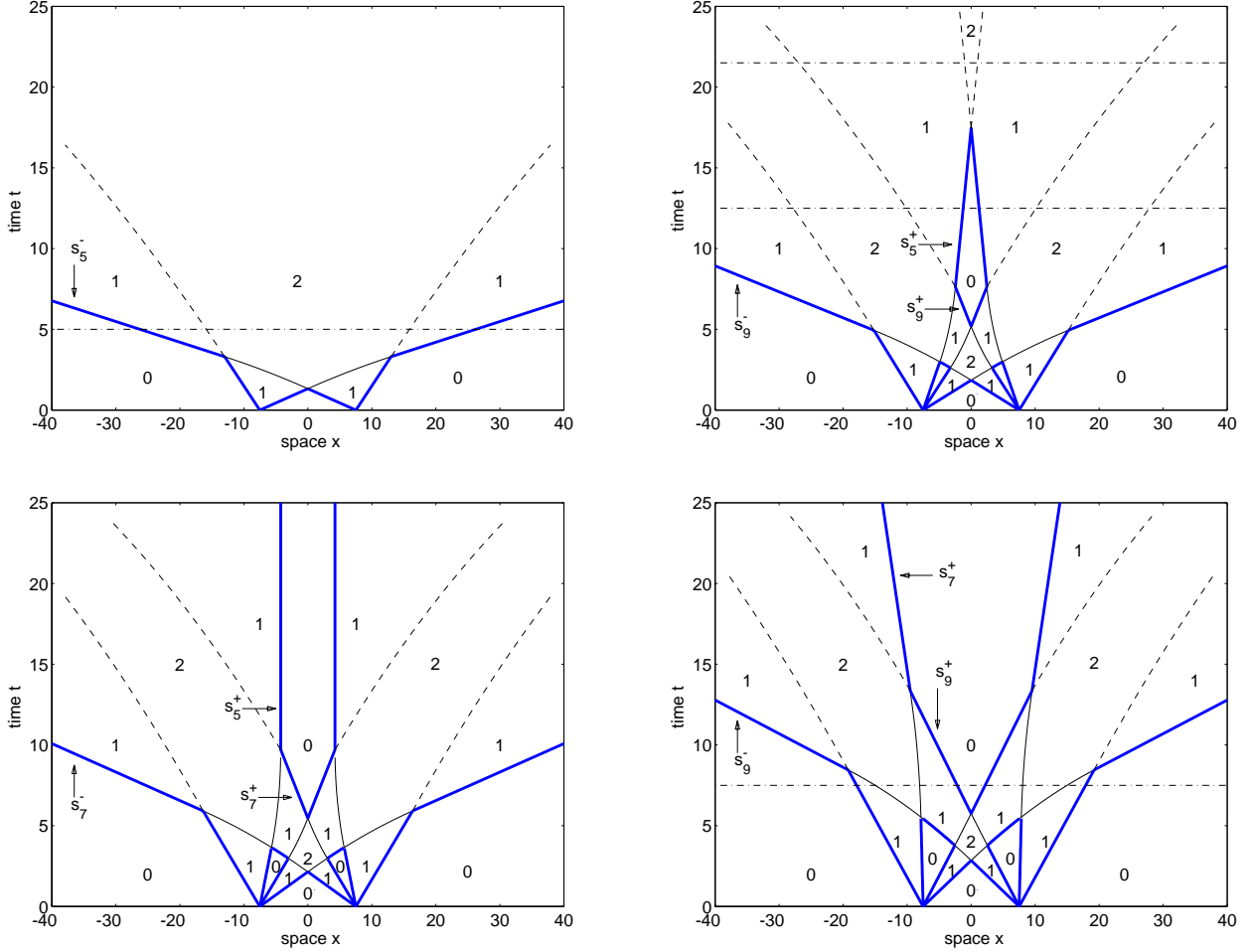


Figure 4.2: Bifurcation diagrams illustrating the regions of genus-0, genus-1 and genus-2 in the (x,t) -plane for the cases shown in Fig. 4.1, namely: (a, top left) $u_0 = 2001/1000$ ($u_0 > 2q_0$), corresponding to case (i) and Fig. 4.1a; (b, top right) $u_0 = 5/4$ ($2q_0 > u_0 > q_0$), corresponding to case (ii) and Figs. 4.1c,d; (c, bottom left) the critical case $u_0 = 1$, which is the separatrix between cases (ii) and (iii); and (d, bottom right) $u_0 = 5/8$ ($q_0 > u_0 > 0$), corresponding to case (iii) and Fig. 4.1b. The horizontal axis is position, x , and the vertical axis is time, t . In all cases, $q_0 = 1$. The thick (blue) lines indicate the boundaries between regions of genus-0 and genus-1 (cf. Propositions 4.4, 4.7 and 4.8). The thin (black) lines indicate boundaries between genus-1 and genus-2 regions, and were computed by approximating them with circular arcs of given starting point and given initial and final slopes. (These conditions determine the circular arc uniquely.) The thin dashed lines indicate boundaries between genus-1 and genus-2 regions in those cases when the final slope is unknown. The dot-dashed horizontal lines indicate the values of t corresponding to the diagrams of the Riemann invariants in Figs. 4.1a–d.

we locally obtain a trivial regularization. That is, near $x = x_*$, the three Riemann invariants r_5 , r_6 and r_7 are reduced to a single invariant $\hat{r}(x, t)$ given by $\hat{r}(x, t) = r_7(x, t)$ for $x < x_*(t)$ and $\hat{r}(x, t) = r_5(x, t)$ for $x > x_*(t)$, and a similar situation arises for r_4 , r_5 and r_6 near $x = x_{**}$. Those trivial regularizations are however necessary in order for all the Riemann invariants to be nonincreasing functions in x (unlike the case in Fig. 2.1a, where trivial ones can be removed).

Conjecture 4.6 *The width of the outermost genus-2 regions present in cases (ii) and (iii) after interaction tends asymptotically to zero.*

In both case (ii) and case (iii), the speeds of the left- and right-boundaries of the genus-2 region in question are respectively given by s_9^+ and s_7^- (cf. Figs 3.2 and 4.2), where as before the superscripts “−” and “+” refer to the values of the Riemann invariants respectively to the left and to the right of their discontinuities at $t = 0$. The fact that the width decreases monotonically and tends asymptotically to a constant follows from the double sorting property of the characteristic velocities. It is not possible, however, to prove whether the asymptotic width is zero without explicitly calculating the speeds of the boundaries between genus-1 and genus-2 regions, which is beyond the scope of this work. (The appearance of this phenomenon was first noted by F.-R. Tian for the case of the KdV-Whitham equations with two jumps^[30].)

Proposition 4.7 *After interaction, the boundary between the outermost genus-1 regions and the surrounding genus-0 regions is given by $x = \pm(x_0 + s_{\text{outer}}t)$, where $s_{\text{outer}} = s_5^-$ in case (i) and $s_{\text{outer}} = s_9^-$ in cases (ii) and (iii). In all these cases, the resulting velocity is*

$$s_{\text{outer}} = (2u_0 + q_0) \left[1 + 2u_0q_0/(2u_0 + q_0)^2 \right]. \quad (4.5)$$

The characteristic speed can be obtained from degenerate $g = 2$ calculations (cf. Appendix A.4). Note however that the appropriate values of s_5^- and s_9^- however can also be obtained from s_3^+ in Eq. (3.1) and s_5^+ in Eq. (3.2) upon $u_0 \rightarrow 2u_0$. (Cf. Figs. 3.2 and 4.1 and discard the Riemann invariants corresponding to degenerate gaps).

Proposition 4.8 *After interaction, the boundary between the innermost genus-0 region and the surrounding genus-1 regions in cases (ii) and (iii) can be written as*

$$x = \pm(x_1 + s_{\text{inner}}^{(1)}t), \quad x = \pm(x_2 + s_{\text{inner}}^{(2)}t), \quad (4.6)$$

respectively for the initial portion and for the final portion, where the characteristic speeds are: $s_{\text{inner}}^{(1)} = s_9^+$ both in case (ii) and case (iii); $s_{\text{inner}}^{(2)} = s_5^+$ in case (ii), and $s_{\text{inner}}^{(2)} = s_7^+$ in case (iii). Furthermore, in both case (ii) and case (iii) the values of these speeds are:

$$s_{\text{inner}}^{(1)} = q_0, \quad s_{\text{inner}}^{(2)} = q_0 - u_0. \quad (4.7)$$

As before, the characteristic speeds can be obtained via degenerate $g = 2$ calculations (see Appendix A.4 for more details). As before, however, the appropriate values of s_5^+ , s_7^+ and s_9^+ can also be obtained from s_5^+ in case (ii) of section 3 upon rescaling $q_0 \rightarrow q_0 + \frac{1}{2}u_0$ and $u_0 \rightarrow 2u_0$. More precisely, neglecting degenerate gaps, the Riemann invariants that determine the value of $s_{\text{inner}}^{(1)} = s_5^+$ in case (ii) and $s_{\text{inner}}^{(1)} = s_7^+$ in case (iii) are obtained from those that determine s_5^+ in Fig. 3.2b upon rescaling $u_0 \rightarrow 2u_0$. (Cf. Figs. 3.2b and 4.1b,c.) Similarly, the Riemann invariants that determine the value of $s_{\text{inner}}^{(2)} = s_9^+$ both in case (ii) and in case (iii) are obtained from those that determine s_5^+ in Fig. 3.2b (case (ii) in section 3) upon rescaling $q_0 \rightarrow q_0 + \frac{1}{2}u_0$. (Again, cf. Figs. 3.2b and 4.1b,c.)

Remark 4.9. Equations (4.5) and (4.7) also describe the motion of the boundaries of the genus-0 regions in the critical case $u_0 = q_0$, upon proper relabeling of the Riemann invariants. In particular, they predict that in the critical case the width of the inner genus-0 region is constant (i.e., $s_{\text{inner}}^{(2)} = 0$).

The above results, and in particular Eqs. (4.5) and (4.7) show that the speed of the boundaries between regions of genus-0 and genus-1 after the individual perturbations have come into contact is significantly altered as a result of the interaction. In other words, the interaction between different genus-1 regions results in significant bending. This can perhaps be best appreciated in the critical case (i.e., $u_0 = q_0$, cf. Fig. 4.2c).

Finally, we note that, as in the case of one frequency jump, all of the above values for the speeds of the boundaries between genus-0 and genus-1 regions agree very well with the results of numerical simulations of the NLS equation, to be discussed in section 6.

5 Behavior of finite-genus solutions: Arbitrary number of jumps

Similar calculations to the ones described in section 4 can be repeated for jumps of arbitrary size and/or when more than two frequency jumps are present. In particular, from the generalization of the above calculations to an arbitrary number of jumps, it is possible to extract some general features. Thus, we consider an initial condition with constant-amplitude and with initial frequency expressed in terms of N frequency jumps each of size C_j and located at $x = X_j$, $j = 1 \dots, N$:

$$u(x, 0) = -C_{\text{tot}}/2 + \sum_{j=1}^k C_j \quad \text{for } X_k < x < X_{k+1}, \quad (5.1)$$

where $X_0 = -\infty$ and $X_{N+1} = \infty$, and where $C_{\text{tot}} = \sum_{j=1}^N C_j = u(\infty, 0) - u(-\infty, 0)$ is the total jump size. The constant frequency offset $C_{\text{tot}}/2$ in $u(x, 0)$ does not affect the qualitative behavior of solution, and is chosen so that the mean frequency of the solution is zero, i.e., so that the mean position of the solution is constant.

For simplicity, hereafter we will limit ourselves to consider a symmetric collection of positive frequency jumps. That is, we will assume that $C_j > 0 \forall j = 1, \dots, N$ and that if a given jump of amplitude $C = C_*$ exists at $x = X_*$, another jump with the same amplitude exists at $x = -X_*$. (Or, in other words, the initial condition $u(x, 0)$ for the frequency possesses reflection symmetry with respect to the origin.) Since $C_j > 0 \forall j = 1, \dots, N$, the analog of Eqs. (4.4) holds:

$$\max_{x \in \mathbb{R}} r_1^0(x) = r_1^0(\infty) = \lim_{x \rightarrow \infty} r_1^0(x) = -2q_0 - C_{\text{tot}}/2, \quad (5.2a)$$

$$\min_{x \in \mathbb{R}} r_2^0(x) = r_2^0(-\infty) = \lim_{x \rightarrow -\infty} r_2^0(x) = 2q_0 + C_{\text{tot}}/2, \quad (5.2b)$$

Note that again $r_1^0(x)$ and $r_2^0(x)$ are the Riemann invariants before regularization. Owing to Eqs. (5.2) and Definition 4.2, a collection of jumps will be super-critical if $C_{\text{tot}} > 2q_0$, sub-critical if $C_{\text{tot}} < 2q_0$ and critical if $C_{\text{tot}} = 2q_0$.

Proposition 5.1 *In the case of N equal frequency jumps each of size $C = 2u_0$, no individual genus-0 regions develop if the jumps are individually super-critical, i.e., $u_0 > 2q_0$.*

Recall that the size of each of the jumps is $2u_0$ and that the jumps are individually super-critical according to Definition 3.1 when the original Riemann invariants overlap at a single location in space, that is, if

$r_2^0(X_j^-) < r_1^0(X_j^+)$ for $j = 1, \dots, N$. The result applies independently of the number of jumps. More in general, however for an arbitrary collection of frequency jumps we have:

Theorem 5.2 *It is possible to obtain arbitrarily large genera for finite times by considering appropriate collections of frequency jumps. However, asymptotically as $t \rightarrow \infty$, the only expanding regions in the solution are of genus-0, genus-1 and genus-2.*

Proof. The result follows directly from Proposition 2.1 (double sorting property of the characteristic speeds). Let us first note that the non-regularized system has two Riemann invariants, and therefore, independently of the behavior at intermediate values of x , the regularized system will have only two non-degenerate branches as $x \rightarrow \pm\infty$, i.e., $r_1^0(x) < r_2^0(x)$. The only topologically distinct ways to connect these two branches are shown in Figs. 5.1a-d (some of these possibilities were also studied in Ref. [10], but not for genus-2 cases), where we have neglected the possible presence of one or more shrinking regions such

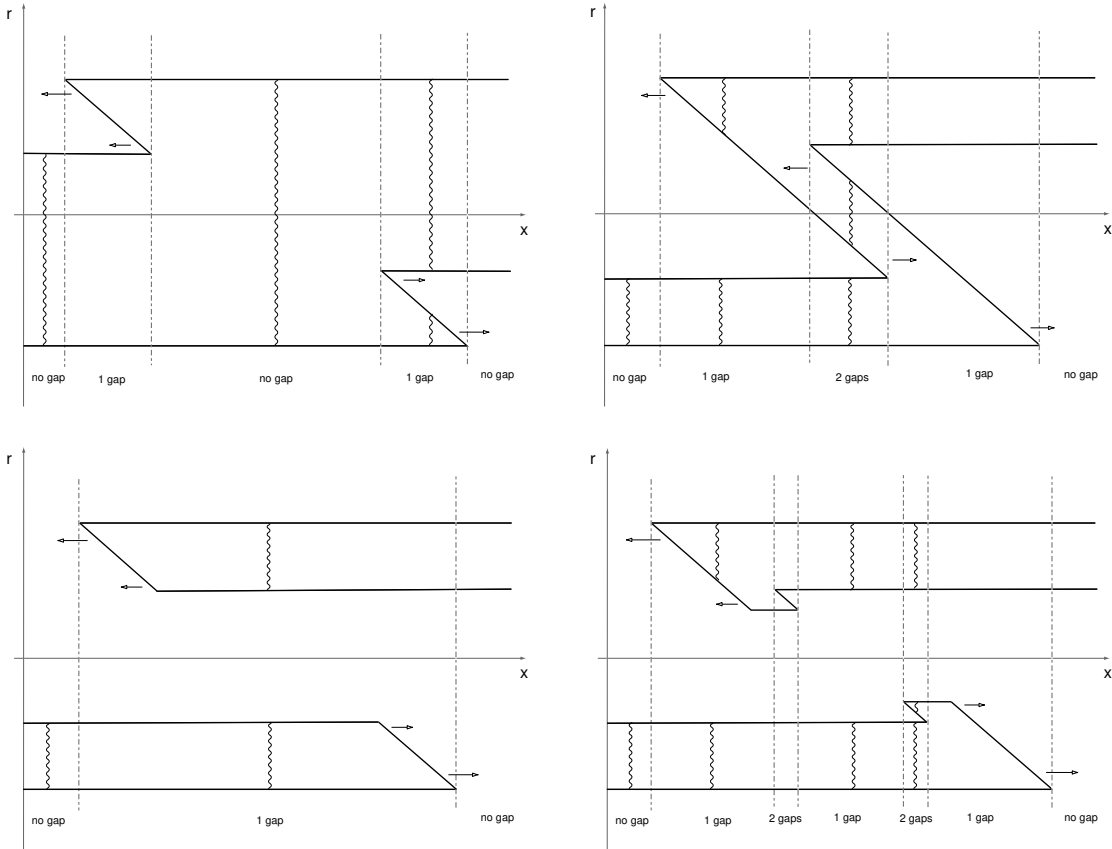


Figure 5.1: Qualitative diagrams illustrating topologically distinct cases for the asymptotic values of the Riemann invariants after removal of the degenerate portions, together with the corresponding separation between regions of genus-0, genus-1 and genus-2: (a, top left) genus-0 region at the center, corresponding to Figs. 3.2b and 4.1b; (b, top right) genus-2 region at the center, corresponding to Fig. 4.1d; (c, bottom left) genus-1 region at the center, corresponding to Fig. 3.2a; and (d, bottom right) originated by a super-critical jump surrounded by sub-critical ones. In each case, the wavy lines show the branch cuts in the Riemann surface $y^2 = \prod_{j=1}^{2g+2} (z - r_j(x, t)) \quad \forall x \in \mathbb{R}$, corresponding to the local spectrum of the Lax operator of the NLS equation.

as the outermost genus-2 regions in Fig. 4.1d (see Remark 5.4 later). The distinction between the different cases in Figs. 5.1a–d is based on the size of the frequency jumps across the pulse. More precisely:

- (i) Fig. 5.1a is obtained when $r_1^0(\infty) < r_2^0(-\infty)$, i.e., when the jumps are collectively sub-critical (as in Figs. 3.2b and 4.1b).
- (ii) Fig. 5.1b is obtained when $r_1^0(\infty) > r_2^0(-\infty)$ but $r_1^0(x^+) < r_2^0(x^-) \forall x \in \mathbb{R}$; that is, when the jumps are collectively super-critical but every jump is individually sub-critical (as in Fig. 3.2d).
- (iii) Fig. 5.1c is obtained when there is only one jump, but that jump is super-critical; that is, a single jump at $x = t_*$, such that $r_1^0(x_*^+) > r_2^0(x_*^-)$ (as in Fig. 3.2a).
- (iv) Fig. 5.1d is obtained when there is one super-critical jump at the center, surrounded by others jumps which are all sub-critical. That is, when there is one jump at $x = 0$ such that $r_1^0(0^+) > r_2^0(0^-)$, surrounded by other jumps at $x = t_j$ such that $r_1^0(x_j^+) < r_2^0(x_j^-) \forall x_j \neq 0$.

Of course, many variations of these basic configurations are possible depending on the details of the arrangement of the frequency jumps. In addition, cases (iii) and (iv) (corresponding to Figs. 5.1c,d), admit a variant in which one or more localized “islands” exist between the two outer portions, as shown in Fig. 5.2a,b (cf. Fig. 4.1a). One of these islands is obtained whenever two additional frequency jumps are inserted which are both individually super-critical, that is, when $r_1^0(x_*^+) > r_2^0(x_*^-)$ for more than one value of $x_* \in \mathbb{R}$. For example, Fig. 5.2a is produced when there are four super-critical jumps (cf. Proposition 5.1); Fig. 5.2b is produced when there are two super-critical jumps surrounded by two sub-critical ones. From these examples it should be clear that the above situations can be easily generalized to cases where an arbitrary number of islands is present by adding a proper number of super-critical frequency jumps. Note that the range of values for the Riemann invariants covered by each of these islands is disjoint from that of all of the other islands. (That is, the islands are not lying side by side. Rather, they are arranged by increasing values of the invariants.) Thanks to the double sorting property possessed by the Riemann invariants (namely, Eqs. (2.4) in Proposition 2.1), islands characterized by larger values of the invariants propagate faster to the left, and therefore, if several islands exist, different islands will temporarily end up stacked on top of each other

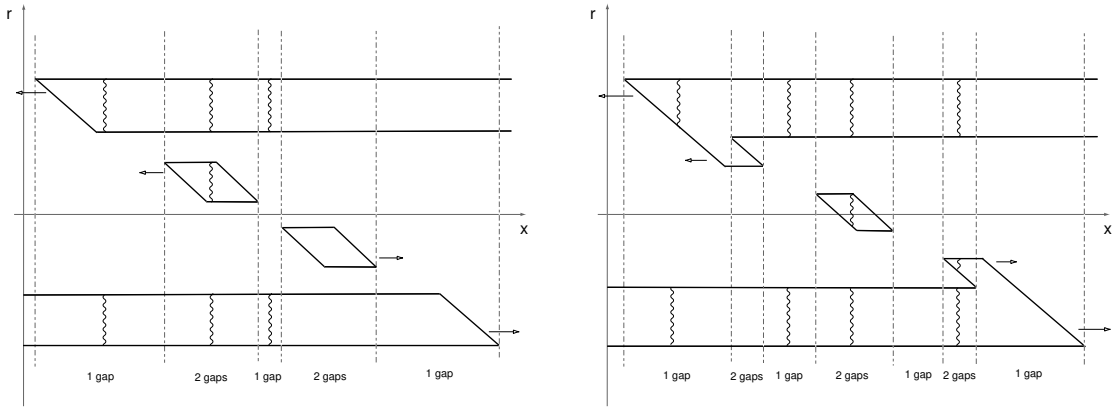


Figure 5.2: Additional diagrams of asymptotic configurations of Riemann invariants, illustrating the possible presence of separate “islands”, each of which produces one additional region of genus-2. Figure 5.2a (left): a variant of Fig. 5.1c corresponding four supercritical jumps. Fig. 5.2b (right): a variant of Fig. 5.1d corresponding to two super-critical jumps surrounded by two sub-critical ones.

upon propagation. It is then clear that by properly choosing the number and size of frequency jumps, it is possible to produce regions of arbitrarily high genus for finite values of t . However, the sorting property of the Riemann invariants also implies that, eventually, each of the islands will separate from the others. Thus, asymptotically in t , at most one island will be present inbetween the top and bottom branches for each value of x , implying that corresponding to each value of x there will be at most two gaps. \square

Remark 5.3. The above decomposition of the solution of the NLS equation (1.1) into regions of genus-0, 1 and 2 asymptotically with time should be compared to the corresponding result for the Korteweg-de Vries (KdV) equation $u_t + 6uu_x + u_{xxx} = 0$, for which it was shown that the solution decomposes into expanding regions of genus-0 and genus-1 asymptotically in time.^[17]

Remark 5.4. It is important to note that regions of genus-3 may also exist in the solution of NLS for all finite values of time. For example, Fig. 5.3a shows the invariants produced by a configuration with two collectively sub-critical jumps surrounded by two individually super-critical ones, while Fig. 5.3b shows the invariants produced by a collection of three jumps which are individually sub-critical but collectively supercritical. Due to the double sorting property of the Riemann invariants, however, the width of these regions decreases monotonically, and tends to a constant asymptotically with time. Therefore, the presence of these regions does not invalidate the statement of Theorem 5.2. Moreover, we expect the width of these genus-3 regions to tend asymptotically to zero with time (cf. Conjecture 4.6). The situation is similar to the case of the KdV equation, where, in addition to expanding regions of genus-0 and genus-1, shrinking regions of genus-2 may also exist asymptotically.

From the proof of Theorem 5.2 we also have:

Corollary 5.5 *Whenever an overall genus-0 region develops at the center of the pulse as a result of the interaction among all frequency jumps, its amplitude is always given by the analogue of Eq. (1.8), namely $\rho_{\max} = \frac{1}{16} (r_2^0(\infty) - r_1^0(-\infty))^2$, in a similar way as for the single-jump case.*

In other words, the above value is the largest amplitude of a genus-0 region that can be achieved with any number N of frequency jumps (cf. Figs. 3.2b and 4.1b,c). In the case of equal frequency jumps of size

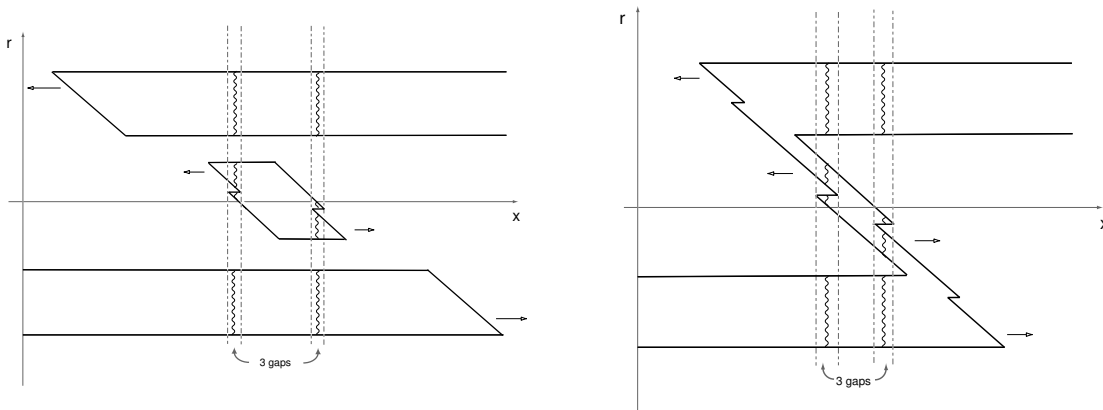


Figure 5.3: Additional diagrams of asymptotic configurations of Riemann invariants showing explicitly the presence of shrinking genus-3 regions; Fig. 5.3a is the analog of Fig. 5.2b; Fig. 5.3b the analog of Fig. 5.1b (see text for details).

$C = 2u_0$, it is $\rho_{\max} = q_0^2(1 + Nu_0/2q_0)^2$.

Corollary 5.6 *Asymptotically as $t \rightarrow \infty$, the solution in the central portion of the pulse will be a region of genus-0 iff the jumps are collectively sub-critical, i.e., iff $r_1^0(\infty) < r_2^0(-\infty)$.*

In the case of equal-size frequency jumps, this condition is satisfied iff $u_0 \leq 2q_0/N$. Thus, the maximum amplitude of a stable genus-0 region is always $\rho_{\max} = 4q_0^2$, again as in the single-jump case, and independently of the number of frequency jumps.

All of the results in this work are relative to initial conditions with constant amplitude and piecewise-constant frequency. If the initial amplitude and frequency vary continuously, some differences can obviously be expected in the solution. Because the quasilinear system of PDEs for the regularized Riemann invariants is always strictly hyperbolic, it is stable with respect to small changes in the initial conditions. Thus, even though the previous results are relative to the case of discontinuous amplitude and frequency jumps, they describe generic features of the solution. Consider for example the dam breaking problem. If the amplitude varies continuously from 0 to its maximum value, oscillations appear near the edges of the pulse. (Indeed, these oscillations are visible in the numerical simulations.) In the absence of frequency jumps, this scenario was studied by Forest and McLaughlin using the Lax-Levermore theory^[14]. As long as the transition region is narrow, however, the amplitude of these oscillations is small, and therefore the solution will bear a close resemblance to the solutions described here. Similar considerations apply if the frequency transitions are not discontinuous, as will be discussed in section 6.

The above results are derived assuming a symmetric collection of positive frequency jumps. The presence of negative frequency jumps at the edges or inbetween other jumps would obviously affect the quantitative details of the picture. We expect that the qualitative features, however, and in particular the asymptotic decomposition into regions of genus-0, 1 and 2, to remain valid.

6 Behavior of finite-genus solutions: Numerical simulations

Even though the analytical calculations described in the previous sections provide a general picture of the behavior of finite genus solutions of the NLS-Whitham equations, there are obviously limits to what can be done analytically. In this section and the following one we therefore complement those analytical results by presenting numerical simulations of the defocusing NLS equation with small dispersion.

All the numerical results presented are obtained by numerically integrating the NLS equation (1.1) with $\varepsilon^2 = 0.1$ using a fourth-order Fourier split-step method. We consider an initial condition $q(x, 0) = |q(x, 0)| \exp[i\varphi(x, 0)/\varepsilon]$, where the initial phase $\varphi(x, 0)$ is obtained by integrating Eq. (5.1):

$$\varphi(x, 0) = \sum_{j=1}^N \left[-x/2 + (x - X_j)H(x - X_j) \right] C_j, \quad (6.1)$$

where the function $H(x) = 1$ if $x \geq 0$ and $H(x) = 0$ if $x < 0$ represents the Heaviside unit step. The initial pulse amplitude was taken to be a super-Gaussian, namely $|q(x, 0)| = q_0 e^{-(x/\Delta X_0)^{2M}}$ with $M = 40$. The integration step size and the width ΔX_0 of the pulse were chosen to be respectively sufficiently small and sufficiently large that none of the numerical results described in this work are affected by them. In order to remove the factor ε in front of the time derivative in Eq. (1.1), the numerical simulations were set-up in terms of the fast scale $t' = t/\varepsilon$. Accordingly, all the numerical results will be described in terms of this time

variable. In what follows we describe the behavior of the solutions for varying values of the parameters X_j and C_j and for varying number of frequency jumps. We first consider the case of two frequency jumps, to numerically identify regions of different genus (Fig. 6.1) and show a few snapshots of the time evolution (Fig. 6.2). We then proceed to describe three sets of simulations: The first set (Fig. 6.3) shows the effect of gradually increasing the size of the frequency jump. The second set (Fig. 6.4) describes the effect of increasing the number of jumps. Finally, the third set (Fig. 6.5) shows the effect of changing the initial separation between these jumps. Although numerical experiments were performed with various values of amplitude, all the figures in this work except Fig. 6.8a are relative to the case $q_0 = 1$.

Two frequency jumps. Figure 6.1 shows contour lines of $|q(x,t)|$ in the (x,t) -plane for different value of the jump size $C_1 = C_2 = 2u_0 =: C$. Because of the finite, non-zero value of ε , not all of the features presented in the previous section are immediately apparent. In other words, because of the finite value of ε , the solution of the NLS equation is only approximately described by a finite-genus solution in each region. Moreover, numerically reconstructing the genus of the solution is a highly nontrivial problem, which is outside the scope of this work. Nonetheless, some regions of genus-0 and genus-1 (whose boundaries have been delimited by dashed lines in Fig. 6.1) are recognizable (e.g., regions of genus-0 are often flat, and therefore appear white in the contour plots in Fig. 6.1), and their location displays a very good qualitative and quantitative agreement with the analytical calculations presented in section 4. Note in particular that, even though the value of ε is not particularly small, the value of C which corresponds to the critical case is exactly that which was predicted analytically, namely $C = 2$. Figure 6.2 shows four snapshots illustrating the evolution with time of the critical case shown in Fig. 6.1c.

It is also interesting to note that the hexagonal patterns visible in Figs. 6.1 (in particular, near the center $x = 0$ in Figs. 6.1a and 6.1b) show the interaction of two counter propagating genus-1 (periodic) waves, which produce, as a result, a genus-2 solution of the NLS equation. Note that in the absence of nonlinearity, a superposition of two simple waves would produce just a parallelogrammic pattern. Thus, the hexagonal pattern is the result of nonlinear phase shifts in the interaction. (Note that the hexagonal pattern can also be found in genus-2 solutions of the Kadomtsev-Petviashvili equation describing two-dimensional shallow water waves^[18].)

Size of the frequency jumps. This set of simulations, some results of which are shown in Fig. 6.3, is relative to a two-jump initial condition. We take the two jumps to be equal-size, $C_1 = C_2 = 2u_0 = C$, and to be initially positioned at $X_1 = X_2 = \pm 2.5$. Looking at the behavior of the solution as C varies, one can clearly observe that the amplitude of the genus-0 portion of the solution increases linearly with increasing value of C . More precisely, $|q|_{\max} = q_0 + C/2$, in agreement with the analytical calculations presented in the previous section (cf. Corollary 5.5). See also Fig. 6.7a later. Moreover, in a similar way as in the single-jump case, one can see that the maximum amplitude of a stable genus-0 region is $|q|_{\max} = 2q_0$. When u_0 is larger than the threshold value q_0 , the genus-0 region eventually disappears, as explained in section 4 and as described in Fig. 4.2b. Unlike the single-jump case, however, one can obtain larger values of ρ for limited times, as shown in Figs. 6.3c,d. Note how, over these shorter times, the amplitude of the genus-0 region is still given by $|q|_{\max} = q_0 + C/2$. Note also, however, that the genus-0 solution closes more rapidly for increasingly large values of C , and, above the threshold $C = 4$ (i.e., $C = q_0$) does not open at all, at least for a fixed value of ΔX . These results are in very good agreement with the analytical calculations described in the previous sections (e.g., see Proposition 5.1 and Corollaries 5.5 and 5.6).

Number of frequency jumps. In this set of simulations, some of which are shown in Fig. 6.4, the number N of frequency jumps was varied, while the size of each jump and their initial spatial separation are kept fixed respectively at $C = 2$ and $\Delta X = 5$. From Fig. 6.4, it is apparent that the amplitude of the genus-0 part also increases linearly with the number of jumps. More precisely, $|q|_{\max} = q_0 + NC/4$, in agreement with the analytical calculations presented in the previous sections (cf. Corollary 5.5). See also Fig. 6.7b later. The genus-0 region, however, will eventually close up if the *total* jump exceeds the same threshold as in the previous case: $C_{\text{tot}} = NC = 4q_0$ (cf. Corollary 5.6). For increasingly larger numbers of jumps, the amplitude

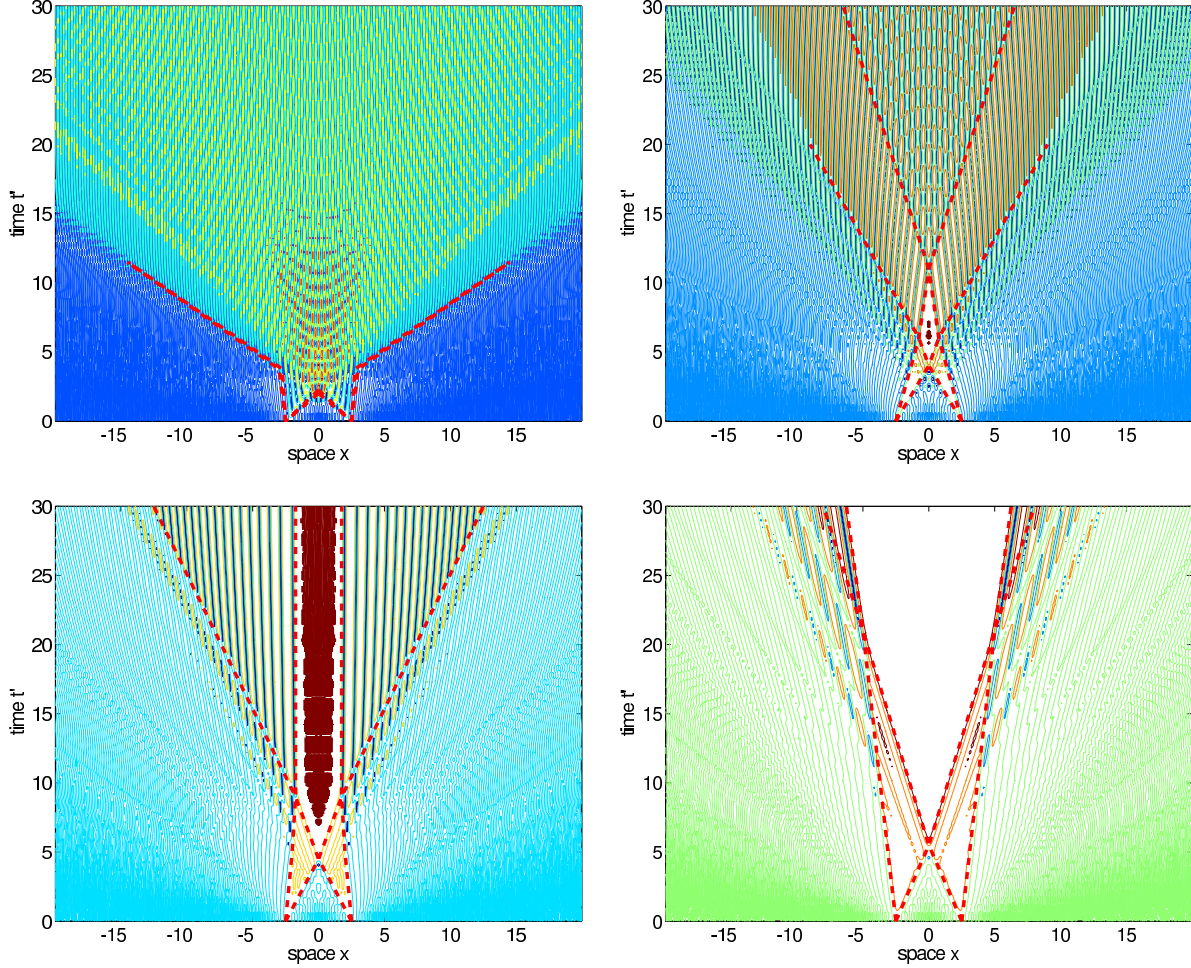


Figure 6.1: Contour plots of numerical simulations of the NLS equation (1.1) for a two-jump initial condition and for different values of the jump size parameter C : (a, top left) $C = 5$, corresponding to Fig. 4.1a and Fig. 4.2a, showing two jumps that are both individually super-critical; (b, top right) $C = 3$ corresponding to Figs. 4.1c,d and Fig. 4.2b, showing two jumps which are individually sub-critical but super-critical in combination; (c, bottom left) the case $C = 2$, corresponding to Fig. 4.2c in which the two jumps are collectively critical; (d, bottom right) $C = 1$, corresponding to Fig. 4.1b and Fig. 4.2d and showing a case in which the jumps are collectively sub-critical. In each case, the dashed lines demarcate the recognizable regions of different genus. In particular, the speeds of the boundaries between genus-0 and genus-1 regions are in very good agreement with the analytical results described in the previous sections.

of the genus-0 region follows the same law as above, namely $|q|_{\max} = q_0 + NC/4$, and can temporarily achieve very large values. The genus-0 region also tends to close up more rapidly, however, and, above a certain number of jumps, does not open at all (at least for a fixed value of ΔX).

Spatial separation between frequency jumps. In this set of simulations we look at the effect of increasing the spatial separation ΔX between the frequency jumps. Figure 6.5 is relative to a two-jump initial condition with $C = 2$. The consequences of changes in ΔX are not as obvious as those of changes in the number of jumps or the jump size. One can see, however, that increasing ΔX has two main effects: on one hand, it lengthens the time scales over which the evolution occurs, since the various regions need to travel for longer distances to come into contact and to interact; at the same time, it determines the width of the stable genus-0 region in the critical case. In fact, numerical results show a remarkable fact, namely that the width X_∞ of the stable genus-0 region depends linearly on the initial spatial separation ΔX between

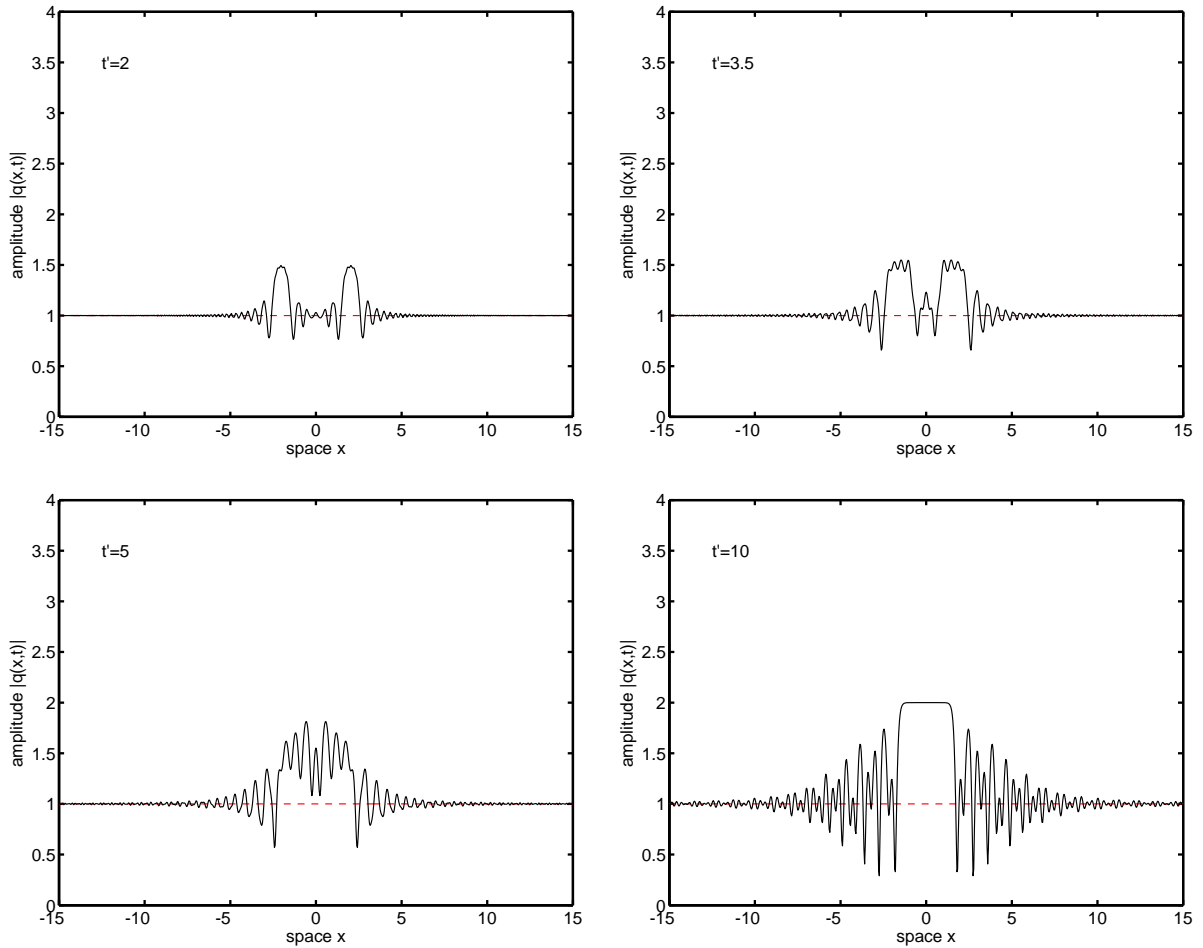


Figure 6.2: Numerical simulations of the NLS equation illustrating the evolution with time of a critical two-jump initial condition. The frequency jumps, located at $X_2 = -X_1 = 5/2$ have amplitude $C_1 = C_2 = 2$, so that their interaction produces a genus-0 region of constant width in the center (as shown in Fig. 6.1c). The solution is shown at: (a, top left) $t' = 2$, (b, top right) $t' = 3.5$, (c, bottom left) $t' = 5$, (d, bottom right) $t' = 10$. This case corresponds to the contour plot in Fig. 6.1c and the bifurcation diagram in Fig. 4.2c.

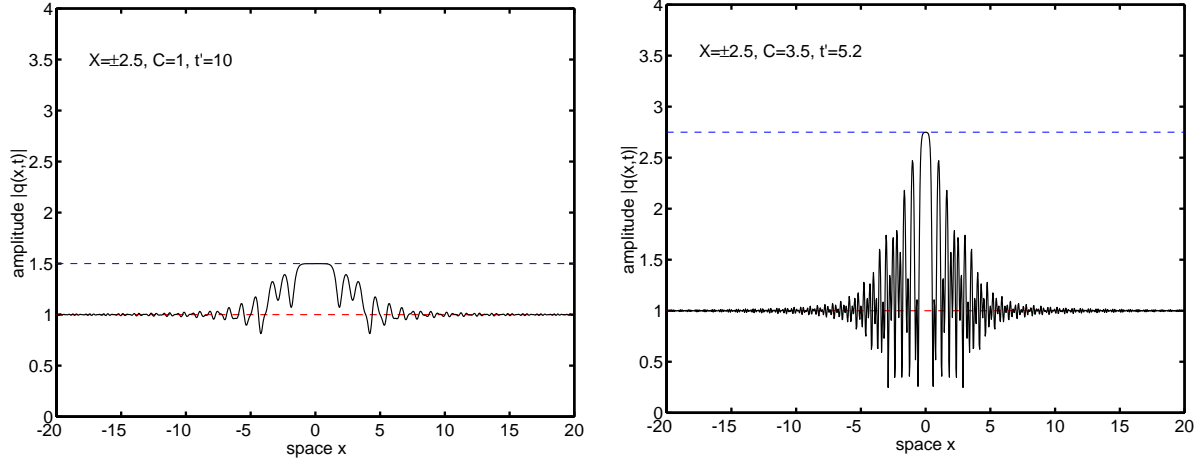


Figure 6.3: Numerical simulations of a two-jump initial condition with $\Delta X = 5$, for different values of the jump size $C_1 = C_2 = C$: (a, left) $C = 1$; (b, right) $C = 7/2$. The critical case $C = 2$ is also shown in Fig. 6.2d. In Fig. 6.3a the solution is subcritical (the genus-0 region expands forever, see Fig. 4.2d), and the solution is shown at $t' = 10$, whereas in Fig. 6.3b the solution is supercritical (see Fig. 4.2b), and it is shown at the time when the genus-0 portion has maximum width, $t' = 5.2$. The horizontal dashed line at $|q| = 1$ represents the amplitude of the initial condition, and the other horizontal dashed line identifies the amplitude of the genus-0 region. Note that: (i) the amplitude of the genus-0 portion of the solution increases linearly with increasing value of C . (ii) for increasingly large values of C , the genus-0 solution tends to close more rapidly, and, above a certain threshold, does not open at all.

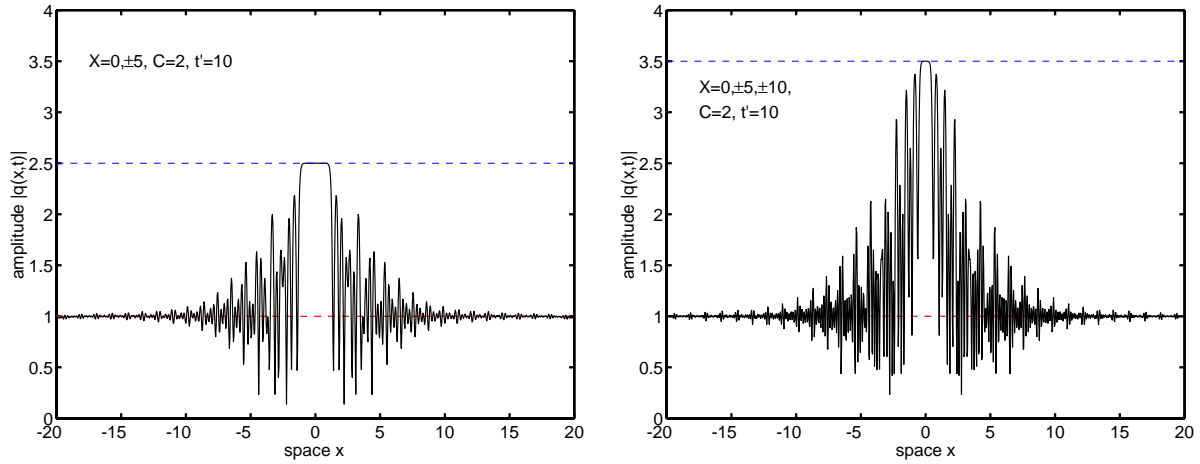


Figure 6.4: Numerical simulations for different numbers N of frequency jumps, with the size of each frequency jump fixed at $C_i = 2$, $i = 1, \dots, N$: (a, left) $N = 3$; (b, right) $N = 5$. In both cases the solution is shown at $t' = 10$. See also Fig. 3.1b, illustrating the case $N = 1$, and Fig. 6.2d, illustrating the (critical) case $N = 2$. Note that for $N = 1$ the central genus-0 region expands and for $N = 2$ it has a steady width, whereas for $N > 2$ it exists only for limited times. In all cases the amplitude of this central genus-0 portion increases linearly with the number of jumps. However, for larger number of jumps, this genus-0 portion tends to close more rapidly, and above a certain number N it does not open at all, at least for a fixed value of ΔX .

the jumps. In the case of two frequency jumps, one simply has $X_\infty = \Delta X/2$. (Cf. Figs. 6.1c, 6.2 and 6.5.) A similar relation however holds independently of the number of jumps. For a critical arrangement of an arbitrary number N of equal-size, equally spaced positive jumps, it is $X_\infty = (N-1)\Delta X/2$, where ΔX is the initial separation between consecutive jumps. (Cf. Fig. 6.6, and note that $(N-1)\Delta X$ is just the distance among the farthest two frequency jumps.) These relations are verified in Figs. 6.8a,b.

Summary. Let us recapitulate for convenience the main results of the numerical experiments discussed in the above paragraphs. Given N positive frequency jumps with individual sizes C_j and separations ΔX_j , we

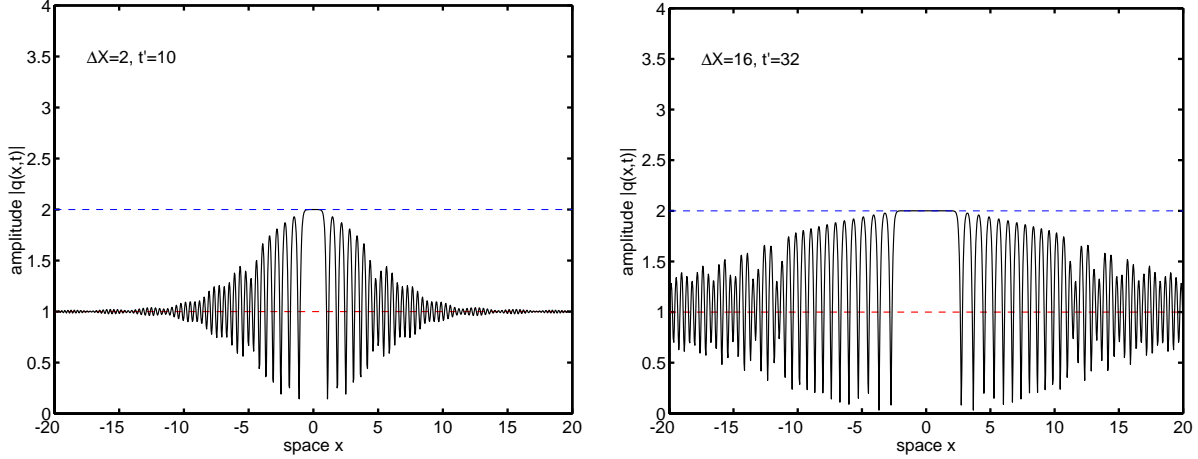


Figure 6.5: Numerical simulations for different separations between jumps, here with a critical arrangement of two frequency jumps of amplitude $C_1 = C_2 = 2$: (a, left) $\Delta X = 2$, (b, right) $\Delta X = 16$. See also Fig. 6.2d, which shows the case $\Delta X = 5$. In Fig. 6.5a the solution is shown at $t' = 10$, in Fig. 6.5b at $t' = 32$. Increasing the value of ΔX has two main effects: it increases the maximum width of the genus-0 portion, and it simultaneously lengthens the time scales over which the evolution occurs. See also Fig. 4.2c.

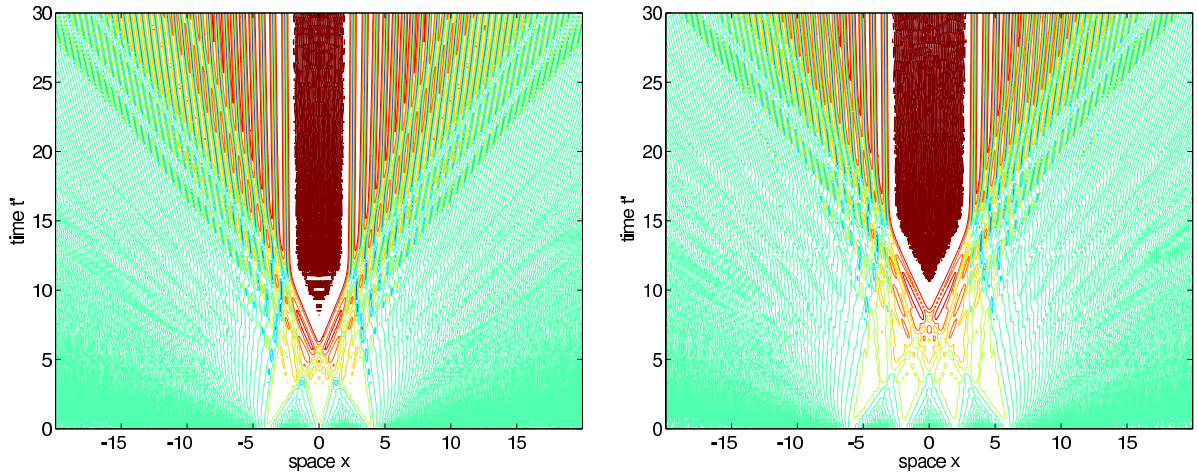


Figure 6.6: Critical arrangements of more than two jumps: (a, left) $N = 3$ and $C = 4/3$; (b, right) $N = 4$ and $C = 1$. In both cases $q_0 = 1$ and $\Delta X = 4$.

can observe that:

- (i) The value of the asymptotic genus in the central portion of the pulse is only determined by the total jump $C_{\text{tot}} = C_1 + \dots + C_N$ (or, equivalently, by the size per jump $C = C_{\text{tot}}/N$ in the case of N jumps of equal size). More precisely, the solution will be genus-0 iff $C_{\text{tot}} < q_0$, in very good agreement with the analytical results (see Corollary 5.6). Of course, the detailed behavior of the solution for finite times depends on the precise values of all the C_j and ΔX_j .
- (ii) If a genus-0 region is desired which expands forever at the center of the pulse, its height is limited by the critical value of the cumulative jump C_{tot} . More precisely, $|q|_{\text{max}} = 2q_0$, independently of the number of jumps. For equal-size jumps, this value is obtained for $C = 4q_0/N$, in very good agreement with the analytical results (see Corollary 5.5).
- (iii) It is possible to achieve genus-0 regions of much larger amplitudes over limited times by employing a sufficiently large number of jumps. More precisely, $|q|_{\text{max}} = q_0 + C_{\text{tot}}/4$ (i.e., $|q|_{\text{max}} = q_0 + NC/4$ for equal-size jumps), as shown in Fig. 6.7, and again in very good agreement with the analytical results (see Corollary 5.5).

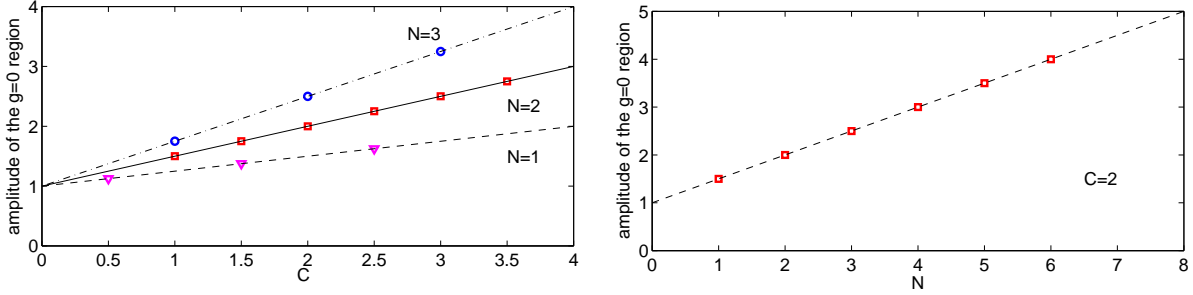


Figure 6.7: (a, left) The numerically calculated amplitude of the genus-0 region produced by an arrangement of N equal-size frequency jumps as a function of the individual jump size C . Triangles: $N = 1$; squares: $N = 2$; circles: $N = 3$. For comparison, the solid, dashed and dot-dashed lines show the straight lines $y = (N - 1)C/4$. (b, right) The amplitude of the genus-0 region produced by an arrangement of frequency jumps each of size $C = 2$, as a function of the number N of jumps. Squares: numerical simulations; dashed line: the line $y = 1 + N/2$.

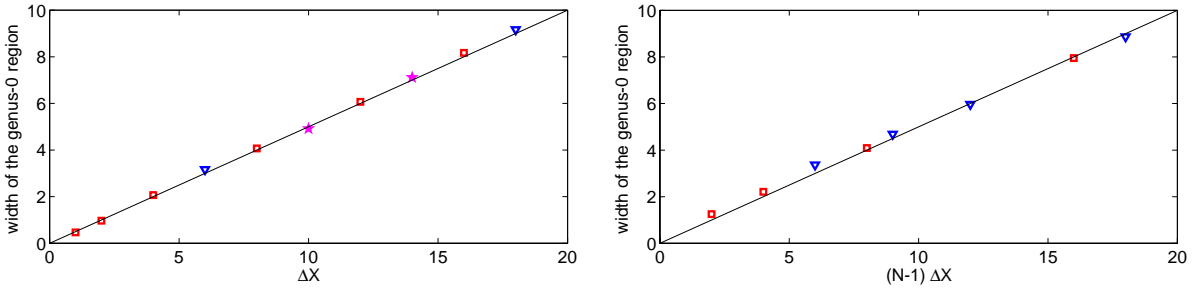


Figure 6.8: Width of the genus-0 region resulting from the interaction of a critical set of frequency jumps as a function of the spatial separation between them: (a, left) $N = 2$; solid line: the straight line $y = \Delta X/2$; squares: simulations with $q_0 = 1$ and $C = 2$; triangles: simulations with $q_0 = 2$ and $C = 4$; stars: simulations with $q_0 = 3$ and $C = 6$. (b, right) $N = 3$ (squares) and $N = 4$ (triangles), with $q_0 = 1$ in both cases; solid line: the straight line $y = (N - 1)\Delta X/2$. Note that, since the characteristic period of the rapid oscillations is $O(\epsilon)$, it is only possible to measure the width of the genus-0 region with precision $\Delta x = \pm \epsilon$.

- (iv) For a critical arrangement of an arbitrary number of equal-size, equally spaced positive frequency jumps, the width of the stable genus-0 region is half of the initial separation between the farthest two frequency jumps. This fact has not been demonstrated analytically, but is nonetheless very solidly supported by the numerical results, as shown in Fig. 6.8.

In the next section we discuss how these results (and in particular items iii and iv) can be used to generate intense, ultra-short optical pulses.

7 Applications: Generation of intense short optical pulses

The analytical and numerical results described in the previous sections can be used to design an initial condition that results in a genus-0 region of arbitrarily high amplitude at any desired distance down the fiber by employing a sufficiently long continuous wave (CW) pulse at the outset, as we now describe. (Recall that, for fiber optics x is the retarded time and t is the propagation distance along the fiber.) Of course, the same techniques can also be applied in any physical context where the dispersionless limit of the NLS equation is relevant. The basic building block consists of two frequency jumps of critical size, which generate a genus-0 region of constant width, as shown in Fig. 6.1c. By including additional frequency jumps to both sides of this basic pair, one can then temporarily produce an overall genus-0 region of higher amplitude. This basic process is illustrated in Fig. 7.1, which shows the time evolution of a four-jump initial condition. A contour plot of this solution is shown in Fig. 7.2a. We now discuss some practical issues related to the generation of these high-intensity pulses: namely, how to control their amplitude, the distance along the fiber at which they are produced, their temporal width, and post-processing through filtering in order to eliminate the high-frequency oscillations.

Amplitude, location and width. By appropriately choosing the number, amplitude and location of the additional frequency jumps, it is possible to precisely specify the amplitude of the overall genus-0 region as well as to prescribe its width and the distance along the fiber at which it is generated. This is illustrated in Fig. 7.2, which contains contours of four different initial conditions. Figure 7.2a corresponds to the four-jump solution shown in Fig. 7.1: the two central frequency jumps are critical ($C_2 = C_3 = 2$), while the single, sub-critical frequency jumps on either side of them ($C_1 = C_4 = 3$) provide two expanding genus-0 regions which go to interact with the main one resulting in an overall genus-0 region of amplitude $|q|_{\max} = q_0 + C_{\text{tot}}/4 = 7/2$, once more in perfect agreement with the analytical prediction.

With similar arrangements of four jumps, one can obtain any value of amplitude $|q|_{\max} < 4$, at which point the two side jumps become critical, and do not generate a genus-0 region anymore. This limitation on the pulse amplitude can be overcome, however, by considering a larger number of frequency jumps. Figures 7.2b,c are both relative to a six-jump initial condition with all jumps having amplitude $C_j = 2$, so that each pair of adjacent jumps generates a genus-0 region of constant width. These regions then interact to create an overall genus-0 region of amplitude 4. In Fig. 7.2b, the jump locations $-X_3 = X_4 = 2$, $-X_2 = X_5 = 15$, $-X_1 = X_6 = 20$ were chosen so that the overall genus-0 region arises near $t' = 15$. In Fig. 7.2c, instead, the side jumps $-X_2 = X_5 = 20$, $-X_1 = X_6 = 35$ were positioned further away, so that the genus-0 region emerges near $t' = 25$ and is maintained for a longer interval. Finally, Fig. 7.2d shows an eight-jump initial condition, with equal-size jumps $C_j = 2$, generating an overall amplitude $|q|_{\max} = 5$. Once more, the jump locations were chosen so that this region emerges near $t' = 25$. A convenient way to choose the

jump locations is to remember that each frequency jump moves with velocity corresponding to the average frequency across the jump.

Finally, we note that the width of the central genus-0 region can be easily adjusted by changing the temporal separation between the two critical frequency jumps, by virtue of the linear relation between these two quantities which was discussed in section 6.

Smooth frequency transitions. The remarks at the end of section 5 about the general stability of the analytical results with respect to small changes in the initial conditions also apply with regard to the discontinuity in the frequency jumps. That is, we expect that the general picture described here will be an approximate description of the pulse behavior even if the frequency transitions were continuous, as would

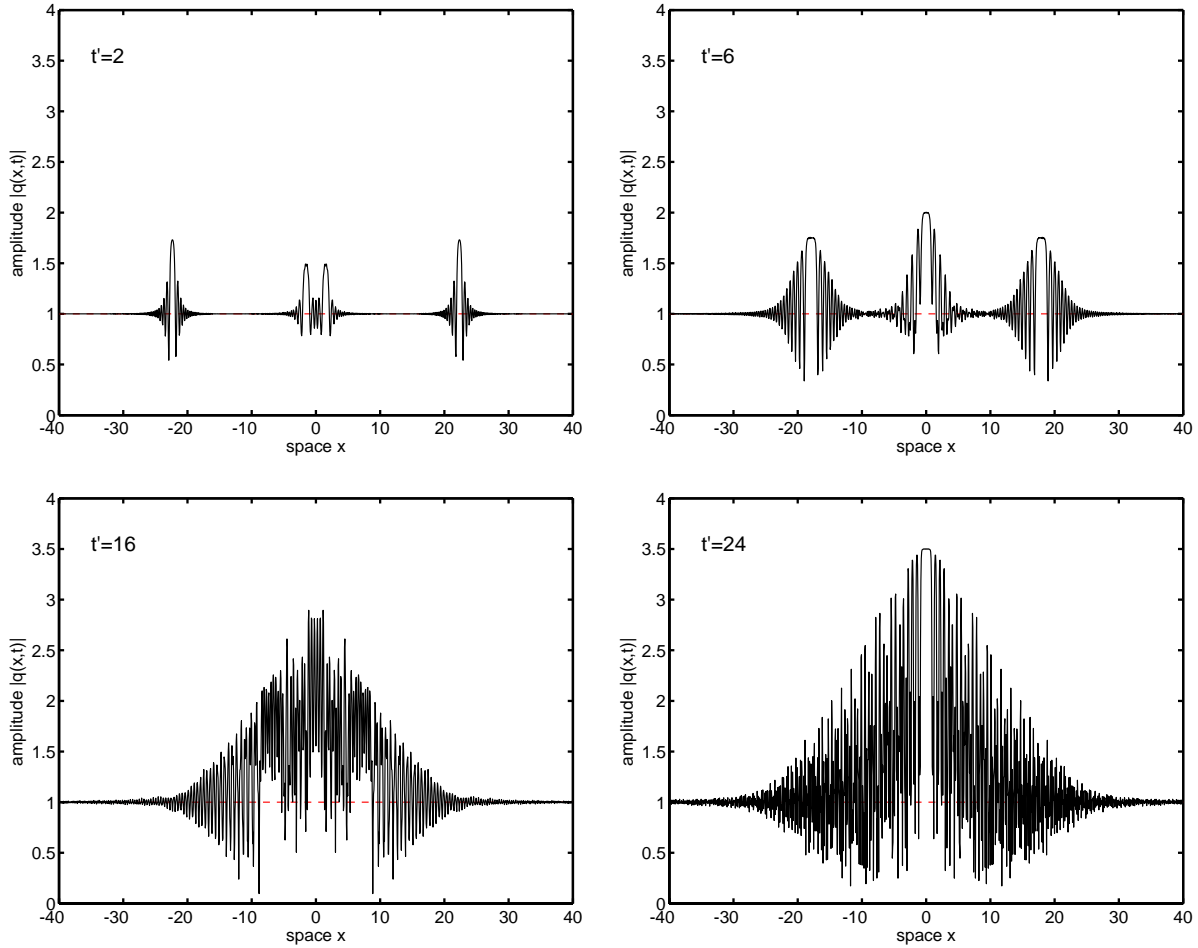


Figure 7.1: Numerical simulations of the NLS equation with a supercritical four-jump initial condition. The frequency jumps, located at $X_4 = -X_1 = 24$ and $X_3 = -X_2 = 2$, have amplitude $C_2 = C_3 = 2$ (so that the interaction of the two center jump produces a critical genus-0 region in the center) and $C_1 = C_4 = 3$, so that the two individual sub-critical jumps open up a genus-0 region which moves towards the center of the pulse. The solution is shown at: (a, top left) $t' = 2$, (b, top right) $t' = 6$, (c, bottom left) $t' = 16$, (d, bottom right) $t' = 24$. A contour plot of this solution is shown in Fig. 7.2a.

be the case in any experimental setup. To test this prediction, we performed numerical simulations in which, instead of Eq. (5.1), the initial frequency was chosen according to

$$u(x,0) = \frac{1}{2} \sum_{j=1}^N C_j \tanh(x - X_j), \quad (7.1)$$

which implies $\varphi(x,0) = (1/2) \sum_{j=1}^N C_j \log(\cosh(x - X_j))$. The comparison of the numerical results for discontinuous and smooth frequency transitions shows remarkable agreement between the two cases, with regard to both the bifurcation diagrams and the the amplitude of the genus-0 regions. As an example, in Fig. 7.3 we show numerical simulations of two frequency jumps with the same parameter values as in Figs. 6.1b–d. Note also that the hexagonal pattern near the center $x = 0$ in Fig. 7.3a shows a genus-2 solution

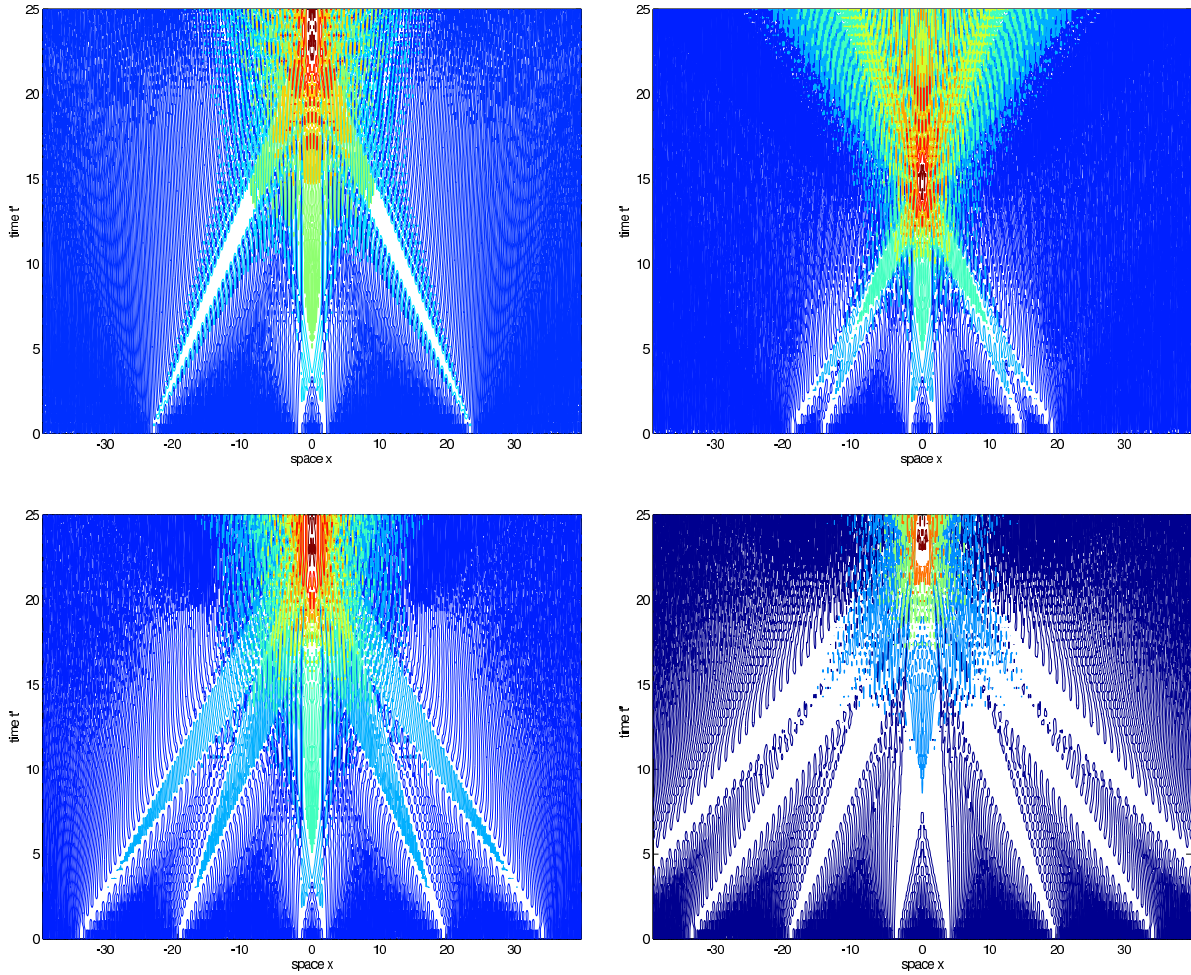


Figure 7.2: Contour plots of the numerical solution of the NLS equation with various choices of frequency jumps: (a, top left) four jumps, with parameters corresponding to the solution shown in Figs. 7.1a–d; (b, top right) six jumps, positioned at $-X_3 = X_4 = 2$, $-X_2 = X_5 = 15$, $-X_1 = X_6 = 20$ and all with amplitude $C = 2$; (c, bottom left) six jumps, with same parameters as before except $-X_2 = X_5 = 20$ and $-X_1 = X_6 = 35$; (d, bottom right) eight jumps, each with amplitude $C = 2$ and positioned at $-X_4 = X_5 = 4$, $-X_3 = X_6 = 20$, $-X_2 = X_7 = 35$, $-X_1 = X_8 = 50$.

of the NLS equation (see also Figs. 6.1). The evolution of the Riemann invariants corresponding to Fig. 7.3a is given by a smooth-version of Fig. 5.1.

Filtering. The high-frequency oscillations that appear on each side of the genus-0 region may be undesirable for practical purposes. These oscillations can be effectively removed by appropriately filtering the pulse at the fiber output, resulting in a smooth, high-amplitude short optical pulse. For example, post-processing with a Lorentzian filter with frequency response $F(\omega) = (\sqrt{R}/\pi)/(1 + R\omega^2)$ with $R \ll 1$ effectively “wipes out” the genus-1 and genus-2 oscillations. A drawback of this method however is that, in the case of a narrow pulse, the conversion efficiency (i.e., the amount of energy in the initial CW pulse that is preserved in the final high-amplitude pulse) is rather low after filtering. A higher conversion efficiency can be obtained either by employing an Erbium-doped fiber amplifier or by increasing the temporal separation between the two central frequency jumps, so as to obtain a wider genus-0 region.

Parameter scaling. As a concluding remark we note that, even though almost all the figures in this work describe solutions produced by initial conditions with amplitude $q_0 = 1$, all of these numerical results can easily be related to different values of initial amplitude thanks to the scaling symmetry of the NLS equation. Namely, if $q(x, t) \rightarrow a q(x, t)$, the results in this work still apply upon rescaling $x \rightarrow x' = x/a$, $t \rightarrow t' = t/a^2$, implying $\rho(x, t) \rightarrow \rho'(x', t') = a^2 \rho(ax', a^2 t')$ and $u(t, x) \rightarrow u'(x', t') = a u(ax', a^2 t')$. Importantly, the same scalings can also be used to relate the results to choices of spatial or temporal units different from those discussed in Appendix A.1.

Acknowledgements

We would like to thank W. L. Kath and M. Fiorentino for providing technical specifications regarding appropriate experimental devices, F.-R. Tian for useful discussions on the Whitham equations and M. Hofer for his careful reading of the text. This work was partially supported by the National Science Foundation under grant numbers DMS-0404931 and DMS-0506101.

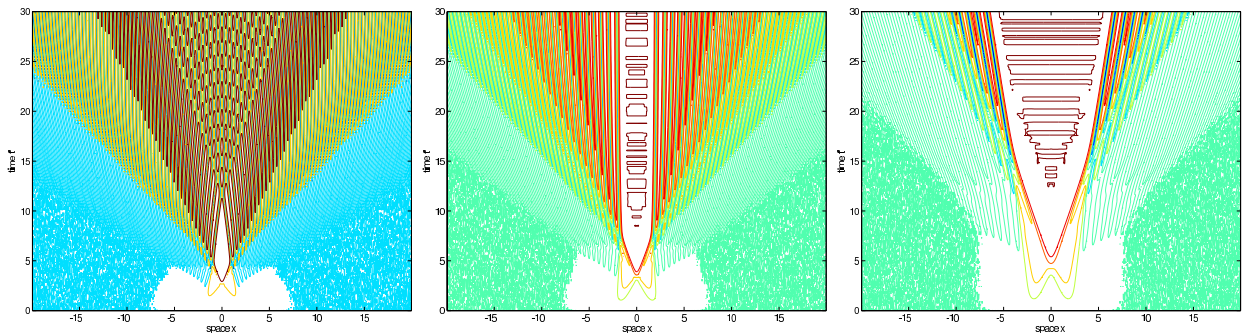


Figure 7.3: Numerical simulations of NLS with smooth frequency transitions, with two frequency jumps located at $X_2 = -X_1 = 2$: (a, left) $C = 3$; (b, center) $C = 2$, (c, right) $C = 1$. These figures should be compared to Figs. 6.1b–d.

Appendix

A.1 Nondimensionalizations and scalings

It has been known for more than thirty years that the propagation of a coherent light pulse in optical fibers is governed by the NLS equation, which, in physical units, is^[4, 21]

$$i\frac{\partial E}{\partial z} - \frac{1}{2}k''\frac{\partial^2 E}{\partial t^2} + \gamma|E|^2E = 0, \quad (\text{A.1})$$

where $E(t, z)$ is the slowly varying amplitude of the complex envelope of the electric field of the pulse, $t = t_{\text{lab}} - z/c_g$ is the retarded time and z is the propagation distance. Here, $c_g = 1/k'$ is the group velocity, $k(\omega)$ the propagation constant, $k'' = d^2k/d\omega^2$ the dispersion coefficient and γ the nonlinear coefficient. In the following, we will use the typical value $\gamma = 3 \text{ W}^{-1}\text{km}^{-1}$.

Introducing the dimensionless variables $q = E/\sqrt{P_*}$, $T = t/t_*$ and $Z = z/z_{\text{nl}}$, where P_* and t_* are some characteristic power and temporal duration, and where $z_* = z_{\text{nl}} = 1/(\gamma P_*)$ is the nonlinear length (the characteristic distance over which nonlinear effects take place), Eq. (A.1) becomes

$$i\frac{\partial q}{\partial Z} - \frac{1}{2}\bar{d}\frac{\partial^2 q}{\partial T^2} + |q|^2q = 0. \quad (\text{A.2})$$

The dimensionless dispersion coefficient $\bar{d} = k''/k_*'' = z_{\text{nl}}/z_{\text{disp}}$ (with $k_*'' = t_*^2/z_{\text{nl}}$) quantifies the relative importance of nonlinear and dispersive effects in Eq. (A.1). In this work we are interested in particular to situations where $0 < \bar{d} \ll 1$. This can be achieved in two different ways: constant dispersion or dispersion management. Note that the dimensionless dispersion coefficient \bar{d} in Eq. (A.2) is obtained equivalently as $\bar{d} = k''/k_*$ or as $\bar{d} = D/D_*$, with $D = -(2\pi c/\lambda^2)k''$, with $D_* = -(2\pi c/\lambda^2)k_*''$, and where D is the dispersion coefficient in $\text{ps}/(\text{nm}\cdot\text{km})$. Note $2\pi c/\lambda^2 = 0.78 (\text{nm}\cdot\text{ps})^{-1}$ at $\lambda = 1.55 \mu\text{m}$.

Typical units. We first consider the case of fibers with constant dispersion. A unit power $P_* = 2 \text{ W}$ (which can be obtained using commercially available high-power Erbium-Doped-Fiber-Amplifier lasers) implies $z_{\text{nl}} = 0.16 \text{ km}$. Then a characteristic time unit of $t_* = 50 \text{ fs}$ (which is appropriate in order to describe short optical pulses) yields $k_*'' = 1.5 \text{ ps}^2/\text{km}$. Then the dimensionless dispersion coefficient \bar{d} in Eq. (A.2) is $\bar{d} = D/D_*$, with $D_* = -1.2 \text{ ps}/(\text{nm}\cdot\text{km})$. A value of $\bar{d} = 0.1$ (such as the one used in all the simulations presented in this work) can then be obtained by employing a fiber with dispersion coefficient $D = -0.12 \text{ ps}/(\text{nm}\cdot\text{km})$. Alternatively, the same effects can be observed for lower-amplitude, longer pulses over longer propagation distances: for example, with a unit power $P_* = 20 \text{ mW}$, and a unit time $t_* = 0.5 \text{ ps}$, the unit distance would be $z_* = 16 \text{ km}$.

Fibers with a larger nonlinear coefficient (such as a dispersion-shifted fiber or a photonic-crystal fiber, for example) would have a correspondingly smaller nonlinear length z_{nl} , which would make it possible to observe the same nonlinear effects over shorter distances. Also, for comparable values of t_* and P_* , a higher nonlinearity would result in a larger value of k_*'' , which means that fibers with correspondingly larger dispersion coefficients may be used. Alternatively, a higher nonlinearity would make it possible to achieve the same value of k_*'' (and hence \bar{d}) with shorter temporal scales t_* and/or with smaller peak powers P_* .

It should be noted that Eq. (A.1) neglects the effect of fiber loss, and therefore the peak powers listed above should be taken as the average of the pulse powers over the whole transmission span. This is not

a serious issue if the total propagation distance is much shorter than the characteristic distances for fiber absorption, as with the sample parameters chosen earlier (for standard telecommunication fibers, a power loss coefficient of 0.2 dB/km is typical), or if the effects of damping can be minimized by placing one or more (Erbium-doped and/or Raman) fiber amplifiers inside the transmission span, since it is well-known that the average dynamics in systems with loss and periodic amplification are still governed by the NLS Eq. (1.1) with constant coefficients.^[19] We should also note that quasi-lossless propagation of optical pulses over several hundred kilometers has recently been achieved by making use of two bidirectional Raman pumps plus fiber Bragg gratings.^[11] Finally, note that Eq. (A.1) also neglects higher-order dispersion. As shown in Ref. [25], third-order dispersion can affect pulse behavior. In order for the results described in this work to apply, therefore, it is necessary that the fiber dispersion be approximately constant throughout the bandwidth of the pulse, which means that third-order dispersion should be small.

Dispersion management. If realizing small values of \bar{d} in a stable way should require an unpractical level of control over fiber dispersion, the problem might be circumvented by making use of dispersion management. With dispersion management, a very small value of ϵ can be achieved as an average between opposite the dispersion coefficients of fibers with alternating signs of dispersion, even if the local values of dispersion are not individually small.

The propagation of optical pulses in systems with dispersion management is still described by the NLS Eq. (A.2), where however the dimensionless dispersion coefficient \bar{d} in Eq. (A.2) is replaced by a periodic function $d(z)$. The specific choice of $d(z)$ is called a dispersion map. The relative effect of the periodic dispersion variations can be quantified by the reduced map strength parameter s which is defined as^[1] $4s = \langle |d(\cdot) - \bar{d}| \rangle_{z_a}$, where now $\bar{d} = \langle d(\cdot) \rangle$ and the average is taken over the period of the dispersion map, z_a . As long as the strength s of the dispersion map is small, it is possible to average over the rapid variations of the pulse profile originating in the NLS equation with periodic coefficients. Indeed, it is well-known that, just like with loss/amplification, the NLS Eq. (A.2) describes the evolution of the leading-order portion of the pulse envelope^[20] in a system with a moderate amount of dispersion management. That is, the leading order part of the pulse satisfies again the NLS equation (A.2), except that the parameter \bar{d} now represents the average dispersion. Therefore, the use of dispersion management might be desirable because it allows one to more easily obtain small values of effective dispersion than for a system with constant dispersion. Because on average the system is still governed by the NLS equation, the results presented in this work will be preserved as long as the dispersion map strength s is small. If the map strength s becomes large, however, the leading order dynamics are described not by the NLS, but rather by a nonlocal evolution equation of NLS-type^[1, 15]. Determining the behavior of the solutions with small \bar{d} for this type of system is a highly non-trivial task, which is beyond the scope of this work.

A.2 Genus-1 solutions of NLS and Whitham's averaging method

Here we briefly review the construction of genus-1 solutions of the NLS equation and the derivation of the genus-1 NLS-Whitham equations, with the aim of clarifying the connection between the Riemann invariants and the spectrum of the Lax operator. For a detailed construction of higher-genus solutions involving theta functions, see Refs. [5, 16].

In order to construct traveling wave solutions of the NLS equation (1.1), it is convenient to introduce the fast space and time scales $x' = x/\epsilon$ and $t' = t/\epsilon$, and write Eq. (1.1) as $iq_{t'} - \frac{1}{2}q_{x'x'} + |q|^2q = 0$. We then look

for solutions of the form

$$q(x', t') = e^{i[cx' + (\frac{1}{2}c^2 + \lambda)t']} (a + f(x' + ct')), \quad (\text{A.3})$$

with $a, c, \lambda \in \mathbb{R}$ and $f(\cdot)$ a real function of its argument. Substituting Eq. (A.3) into NLS and integrating once, one obtains

$$(f')^2 = f^4 - \sigma_1 f^3 + \sigma_2 f^2 - \sigma_3 f + \sigma_4 =: \mu(f), \quad (\text{A.4})$$

where the prime denotes differentiation with respect to x' , $\sigma_1 = -a$, $\sigma_2 = 4(3a^2 - \lambda + c^2/2)$, $\sigma_3 = -a\sigma_2$, $\sigma_4 = C$ and C is the integration constant. It is convenient to represent the right-hand side of Eq. (A.4) as

$$\mu(f) = (f - r_1)(f - r_2)(f - r_3)(f - r_4), \quad (\text{A.5})$$

where the roots r_1, \dots, r_4 are related to the coefficients in Eq. (A.4) via the relations

$$\sigma_1 = r_1 + r_2 + r_3 + r_4, \quad \sigma_2 = r_1 r_2 + r_1 r_3 + r_1 r_4 + r_2 r_3 + r_2 r_4 + r_3 r_4, \quad (\text{A.6a})$$

$$\sigma_3 = r_1 r_2 r_3 + r_1 r_2 r_4 + r_1 r_3 r_4 + r_2 r_3 r_4, \quad \sigma_4 = r_1 r_2 r_3 r_4. \quad (\text{A.6b})$$

Integrating formally Eq. (A.4) one has $\int df / \sqrt{\mu(f)} = \pm(x' - x'_0)$. The integral then defines the solution of NLS in terms of elliptic functions. Note however that real solutions are confined to those values of f such that $\mu(f) > 0$. It is then clear that the values of the four roots r_1, \dots, r_4 (which will be the Riemann invariants when performing the Whitham averaging described in the next subsection) determine the edges of the forbidden regions, or gaps, which are the values of f for which $\mu(f) < 0$. Several situations can occur depending on the values of the parameters in Eq. (A.4); it is relatively easy however to see that bounded solutions only exist when all four roots of $\mu(f)$ are real. In this case, labeling the roots as $r_1 < r_2 < r_3 < r_4$ without loss of generality, $f(x')$ is given by the elliptic sine: $f(x') = k \operatorname{sn}(x', k)$, where the elliptic modulus $k \in [0, 1]$ is given by $k^2 = (r_4 - r_3)(r_2 - r_1) / [(r_4 - r_2)(r_3 - r_1)]$. The elliptic parameter^[3] is $m = k^2$. The value of f oscillates between r_2 and r_3 , and the spatial period of the solution is given by $4K(k)$, where $K(k)$ is the elliptic integral of the first kind.^[3] In the limiting case $r_4 = r_3 = -r_1 = -r_2$, the period of the solution tends to infinity, and one obtains the dark soliton solutions of NLS: for example, when $k = 0$ it is $a = 0$ and $f(x') = \lambda \tanh(\lambda x')$. Note that the solution of NLS is completely specified up to an overall phase in terms of the four roots r_1, \dots, r_4 . For a more detailed discussion of single-phase solutions of the NLS equation in the focusing as well as defocusing regimes, as well as their stability, see Refs. [8, 24].

It is important to note that, for any finite value of the small parameter ε , the presence of ε in Eq. (1.1) can be taken into account by simply replacing (x, t) by the fast variables $(x' = x/\varepsilon, t' = t/\varepsilon)$. This phenomenon is the origin of the high-frequency oscillations in the solution of NLS with small dispersion coefficient, discussed throughout this work. The nontrivial issue, however, is to understand the qualitative behavior of the solution in the weak dispersion limit, as formulated in section 1.

Let us then briefly outline how to obtain the genus-1 NLS-Whitham equations. It is well-known that the NLS equation admits an infinite number of conservation laws:

$$\frac{\partial F_n}{\partial t'} = \frac{\partial G_n}{\partial x'}, \quad (\text{A.7})$$

$n = 1, \dots, \infty$. For example, the first four conserved densities are

$$F_1 = |q|^2, \quad (\text{A.8a})$$

$$F_2 = i(q^* q_{x'} - q q_{x'}^*), \quad (\text{A.8b})$$

$$F_3 = |q_{x'}|^2 + |q|^4, \quad (\text{A.8c})$$

$$F_4 = i(q^* q_{x'x'x'} - q q_{x'x'x'}^*) - 3i|q|^2(q^* q_{x'} - q q_{x'}^*). \quad (\text{A.8d})$$

Then we consider small modulations of the genus-1 solution given by the elliptic function, in the sense that the deformation due to the modulation is of order ε over one period of the wave. Following the standard perturbation method of multiple scales, we introduce the slow time and space scales $x = \varepsilon x'$ and $t = \varepsilon t'$. We now have two sets of scales, consisting of a set of fast scales for the oscillations and a set of slow scales for the modulations. With those variables, we have

$$\frac{\partial}{\partial x'} \rightarrow \frac{\partial}{\partial x'} + \varepsilon \frac{\partial}{\partial x}, \quad \frac{\partial}{\partial t'} \rightarrow \frac{\partial}{\partial t'} + \varepsilon \frac{\partial}{\partial t}.$$

Then, expanding the conserved quantities as $F_n = F_n^0 + \varepsilon F_n^1 + \dots$ and $G_n = G_n^0 + \varepsilon G_n^1 + \dots$ and taking the average of the conservation laws (A.7) over the fast scale x' , at order ε we obtain the NLS-Whitham equations in conservation form:

$$\frac{\partial \langle F_n^0 \rangle}{\partial t} = \frac{\partial \langle G_n^0 \rangle}{\partial x}. \quad (\text{A.9})$$

Here $\langle F_n^0 \rangle$ and $\langle G_n^0 \rangle$ are the average of the leading order conserved densities and fluxes associated with the solution of the NLS equation, and the average of a periodic function $f(x', t') = \hat{f}(\theta)$ is given by

$$\langle f \rangle = \frac{1}{L} \int_{-L/2}^{L/2} f(x', t') dx' = \int_0^1 \hat{f}(\theta) d\theta, \quad (\text{A.10})$$

where L is the spatial period and $\theta = (x' + ct')/L$. For the genus-1 solutions described above, $L = 4K(k)$. Note that the averaged quantities $\langle F_n^0 \rangle$ and $\langle G_n^0 \rangle$ are functions of the spectral parameters r_1, \dots, r_4 . Thus the modulations are expressed in terms of the slow motion of the spectral parameters r_1, \dots, r_4 . This also means that we need the first four equations from (A.9). By computing the averages, one finds that the variables r_1, \dots, r_4 are precisely the Riemann invariants for the system. Then, by writing Eqs. (A.9) in diagonal form, one finally obtains the genus-1 NLS-Whitham equations (2.3) with $g = 1$. (That Eqs. (A.9) are diagonalizable is not obvious, but always true for all values of genus; see section A.3 for further details.)

A.3 The NLS-Whitham equations

Here we briefly review some well-known results for the NLS-Whitham equations. For more details on the finite genus solutions of the NLS equation, the averaging process and the NLS-Whitham equations, we refer the reader to Refs. [5, 25] and references therein.

The genus- g NLS-Whitham equations can be obtained by extending the approach described in section A.2 to hyper-elliptic solutions of NLS and $2g + 2$ conservation laws^[13]. It is more convenient, however, to take advantage of the integrable structure of the NLS equation, as described in Ref. [25]. Recall that genus- g solutions of NLS are associated to the Riemann surface $R: w^2 = \mu_g(z)$, where $\mu_g(z) = \prod_{k=1}^{2g+2} (z - r_k)$ (cf. Eq. (2.2)). It was shown in Refs. [12, 13, 27, 29] that the NLS-Whitham equations (A.9) can be elegantly written as

$$\frac{\partial \omega_1}{\partial t} = \frac{\partial \omega_2}{\partial x}, \quad (\text{A.11})$$

where ω_1 and ω_2 are the meromorphic (Abelian) differentials of the second kind associated with the Rie-

mann surface R :

$$\omega_1 = \frac{1}{2} \left[1 + \frac{z^{g+1} - \frac{1}{2}\sigma_1 z^g + \alpha_1 z^{g-1} + \dots + \alpha_{g-1} z + \alpha_g}{\sqrt{\mu_g(z)}} \right] dz = (1 + O(1/z)) dz, \quad (\text{A.12a})$$

$$\omega_2 = \frac{1}{2} \left[z + \frac{z^{g+2} - \frac{1}{2}\sigma_1 z^{g+1} + \frac{1}{2}(\sigma_2 - \frac{1}{4}\sigma_1^2) z^g + \gamma_1 z^{g-1} + \dots + \gamma_{g-1} z + \gamma_g}{\sqrt{\mu_g(z)}} \right] dz = (z + O(1/z)) dz, \quad (\text{A.12b})$$

where $\sigma_1, \dots, \sigma_3$ are the generalization of Eqs. (A.6),

$$\sigma_1 = \sum_{1 \leq j \leq 2g+2} r_j, \quad \sigma_2 = \sum_{1 \leq j < k \leq 2g+2} r_j r_k, \quad \sigma_3 = \sum_{1 \leq i < j < k \leq 2g+2} r_i r_j r_k \quad (\text{A.13})$$

(σ_3 will appear later on) and where the coefficients α_j and γ_j are given by the solution of two $g \times g$ linear systems of equations

$$I_j^{g+1} - \frac{1}{2}\sigma_1 I_j^g + \alpha_1 I_j^{g-1} + \dots + \alpha_{g-1} I_j^1 + \alpha_g I_j^0 = 0, \quad (\text{A.14a})$$

$$I_j^{g+2} - \frac{1}{2}\sigma_1 I_j^{g+1} + \frac{1}{2}(\sigma_2 - \frac{1}{4}\sigma_1^2) I_j^g + \gamma_1 I_j^{g-1} + \dots + \gamma_{g-1} I_j^1 + \gamma_g I_j^0 = 0, \quad (\text{A.14b})$$

$j = 1, \dots, g$, with the real-valued functions I_j^k given by

$$I_j^k = \frac{1}{2} \int_{r_{2j+1}}^{r_{2j+2}} \frac{z^k}{\sqrt{-\mu_g(z)}} dz. \quad (\text{A.15})$$

Equations (A.14) express the requirement that the A-periods of ω_1, ω_2 be zero: that is, $\oint_{a_j} \omega_1 = \oint_{a_j} \omega_2 = 0$, where the a_j are the A-cycles on the Riemann surface R .

Evaluating the residue of $\omega_{1,2}$ at $z = r_k$ in Eq. (A.11), one obtains the genus- g NLS-Whitham equations in Riemann invariant form:

$$\frac{\partial r_k}{\partial t'} = s_k(r_1, \dots, r_{2g+2}) \frac{\partial r_k}{\partial x}, \quad (\text{A.16})$$

$k = 1, \dots, 2g+2$. The characteristic speeds are given by $s_k(r_1, \dots, r_{2g+2}) = s(r_k)$, with

$$s(r) = \frac{r^{g+2} - \frac{1}{2}\sigma_1 r^{g+1} + \frac{1}{2}(\sigma_2 - \frac{1}{4}\sigma_1^2) r^g + \gamma_1 r^{g-1} + \dots + \gamma_{g-1} r + \gamma_g}{r^{g+1} - \frac{1}{2}\sigma_1 r^g + \alpha_1 r^{g-1} + \dots + \alpha_{g-1} r + \alpha_g}. \quad (\text{A.17})$$

Since the NLS-Whitham equations (A.16) describe the evolution of the Riemann invariants r_1, \dots, r_{2g+2} with respect to the slow time and space variables, and since the Riemann invariants are also the branch points of the Riemann surface corresponding to finite-genus solutions of the NLS equation, it follows that the NLS-Whitham equations describe the slow modulation of finite-genus solutions of the NLS equation.

Note that the abelian differentials in Eqs. (A.12) can also be expanded in terms of the conservation laws of the NLS equation:

$$\omega_1 \sim \left(1 + \sum_{n=1}^{\infty} \frac{n \langle F_n^0 \rangle}{z^{n+1}} \right) dz, \quad \omega_2 \sim \left(z + \sum_{n=1}^{\infty} \frac{n \langle G_n^0 \rangle}{z^{n+1}} \right) dz, \quad (\text{A.18})$$

where $\langle F_n^0 \rangle$ and $\langle G_n^0 \rangle$ are the conserved densities and fluxes of the NLS equation, averaged over the fast phases. The average of a quasi-periodic function of g phases $f(x', t') = \hat{f}(\theta_1, \dots, \theta_g)$, with $\theta_k = (x' + c_k t')/L_k$ and L_k being the period for the phase θ_k , is given by

$$\langle f \rangle = \lim_{L \rightarrow \infty} \frac{1}{L} \int_{-L/2}^{L/2} f(x', t') dx' = \int_0^1 \cdots \int_0^1 \hat{f}(\theta_1, \dots, \theta_g) d\theta_1 \cdots d\theta_g,$$

where we have used the ergodic assumption, i.e., that the g phases produce a dense orbit on the Jacobian variety of the Riemann surface^[12]. In this framework Eqs. (A.11) then yield Eqs. (A.9) for $n = 1, \dots, 2g + 2$. For example, the first few densities and fluxes are

$$\begin{aligned} \langle F_1^0 \rangle &= \langle \rho \rangle = -\frac{1}{4}\sigma_2 + \frac{1}{16}\sigma_1^2 + \frac{1}{2}\alpha_1, \\ \langle F_2^0 \rangle &= \langle \rho u \rangle = -\frac{1}{4}\sigma_3 - \frac{1}{8}\sigma_1\sigma_2 + \frac{1}{32}\sigma_1^3 + \frac{1}{8}\sigma_1\alpha_1 + \frac{1}{4}\alpha_2, \\ \langle G_1^0 \rangle &= \langle F_2^0 \rangle = -\frac{1}{4}\sigma_3 - \frac{1}{8}\sigma_1\sigma_2 + \frac{1}{32}\sigma_1^3 + \frac{1}{2}\gamma_1, \\ \langle G_2^0 \rangle &= \langle \rho u^2 + \frac{1}{2}\rho^2 \rangle = -\frac{1}{8}\sigma_4 + \frac{1}{8}\sigma_1\sigma_3 + \frac{1}{32}\sigma_2^2 - \frac{5}{64}\sigma_1^2\sigma_2 + \frac{9}{512}\sigma_1^4 + \frac{1}{8}\sigma_1\gamma_1 + \frac{1}{4}\gamma_2, \end{aligned}$$

and Eq. (1.5) is obtained from Eqs. (A.9) when $g = 0$.

Upon evaluating the integrals in Eq. (A.15) and taking the appropriate limits as $\varepsilon \rightarrow 0^+$, Eq. (A.17) can be used to calculate the value of all the speeds listed in sections 3 and 4, as we show in the next subsection. It should be noted that the general solution of the NLS-Whitham equations (A.16) can be written in terms of the Hodograph transformation

$$x - s_k(r_1, \dots, r_{2g+2})t = w_k(r_1, \dots, r_{2g+2}), \quad (\text{A.20})$$

$k = 1, \dots, 2g + 2$, where the functions w_k are expressed in terms of the initial data via hyperelliptic integrals. When inverting Eqs. (A.20) to find the solution $q(x, t)$, the locations where the Jacobian of the transformation vanishes determine the boundary between regions of different genus^[31, 32]. This information was used in Ref. [31] to determine the location between regions of genus-0 and genus-1 in some specific situations, and the method was used in Ref. [17] to determine the generic evolution of an arbitrary initial datum for the Korteweg-de Vries equation. It should be noted, however, that the method cannot be easily applied for the situations considered in the present work, since the transformation $x \rightarrow q(x, 0)$ is not invertible in the case of piecewise constant initial data, which are the ones of interest here.

A.4 Calculation of some characteristic speeds

We now briefly describe some calculations regarding the characteristic speeds of the regularized Riemann invariants for the NLS-Whitham equations. The results of these calculations and similar others were summarized in sections 3 and 4. Since the calculations are rather tedious however, we will limit ourselves to present two examples. For more details on similar types of calculations we also refer the reader to Refs. [7, 25]. When performing these calculations, it is useful to note that the characteristic speed in Eq. (A.17) is the ratio of two meromorphic differentials which becomes the ratio of two polynomials (the denominator of the differentials). In the case of step initial data, some common factors then arise, and the resulting cancellations produce a finite result.

Genus-1 calculations: Equations (3.1) and (4.5). Our first aim is to calculate s_3^- in case (i) of section 3, as shown in Fig. 3.2a. This is done by evaluating $s_3(r_1, \dots, r_4) = s(r_3)$, with $s(r)$ given by Eq. (A.17) with $r_4 = -r_1 = u_0 + 2q_0$, $r_2 = -u_0 + 2q_0$ and $r_3 = r_4 - \varepsilon$, and then taking the limit $\varepsilon \rightarrow 0^+$. In general, Eqs. (A.14) yield the coefficients α_1 and γ_1 for the $g = 1$ case as

$$\alpha_1 = -\frac{I_1^2 - \frac{1}{2}\sigma_1 I_1^1}{I_1^0}, \quad \gamma_1 = -\frac{I_1^3 - \frac{1}{2}\sigma_1 I_1^2 + \frac{1}{2}(\sigma_2 - \frac{1}{4}\sigma_1^2)I_1^1}{I_1^0}. \quad (\text{A.21})$$

In our case, Eqs. (A.13) also give $\sigma_1 = r_2 + r_4 = 4q_0 + \varepsilon$ and $\sigma_2 = r_2 r_4 - r_3^2 = -2u_0(u_0 + 2q_0) + \varepsilon(u_0 - 2q_0)$. In general, upon making the substitution $z = r_3 + \Delta \sin^2 \theta$ with $\Delta = r_4 - r_3$, the integrals I_1^0, \dots, I_1^3 take the convenient form:

$$I_1^k = \int_0^{\pi/2} \frac{(r_3 + \Delta \sin^2 \theta)^k}{\sqrt{(r_3 - r_1 + \Delta \sin^2 \theta)(r_3 - r_2 - \Delta \sin^2 \theta)}} d\theta. \quad (\text{A.22})$$

In our case, expanding the power in the numerator and substituting the explicit value of the invariants, the integrals can also be written as:

$$I_1^k = \sum_{m=0}^k \binom{k}{m} (u_0 + 2q_0)^{k-m} \varepsilon^m \int_0^{\pi/2} \frac{\sin^{2m} \theta}{\sqrt{(2(u_0 + 2q_0) - \varepsilon \cos^2 \theta)(2u_0 - \varepsilon \cos^2 \theta)}} d\theta. \quad (\text{A.23})$$

Then, evaluating the integrals in Eq. (A.23), substituting the results and Eq. (A.21) into Eq. (A.17) and taking the limit $\varepsilon \rightarrow 0^+$, one then obtains the desired result, namely Eq. (3.1). Note that, even though $\lim_{\varepsilon \rightarrow 0^+} I_1^0 = \infty$, the final result for the characteristic speed is finite.

We should emphasize that, by rescaling $u_0 \rightarrow 2u_0$, the above calculation also provides the speed s_{outer} in Eq. (4.5) of section 4. More precisely, upon neglecting degenerate branches in Figs. 4.1a–c, the values of the Riemann invariants that determine s_3^- in Fig. 3.2a are exactly those of the Riemann invariants that determine s_5^- in case (i) (cf. Fig. 4.1a) and s_9^- in cases (ii) and (iii) (cf. Figs. 4.1b,c) of section 4 upon replacing $u_0 \rightarrow 2u_0$.

Degenerate genus-2 calculations: Equations (3.2) and (4.8). We now want to calculate s_5^+ in case (ii) of section 3, as shown in Fig. 3.2b. This is done by evaluating $s_5(r_1, \dots, r_6) = s(r_5)$, with $s(r)$ still given by Eq. (A.17) with $g = 2$ and with $r_6 = -r_1 = u_0 + 2q_0$, $r_4 = -r_3 = -u_0 + 2q_0$, $r_5 = -r_2 = r_4 + \varepsilon$, and then taking again the limit $\varepsilon \rightarrow 0^+$. In general, Eqs. (A.14) yield the coefficients α_1 , α_2 , γ_1 and γ_2 for the $g = 2$ case as:

$$\alpha_{j+1} = (-1)^{j+1} \frac{1}{[1, 0]} \left([3, j] - \frac{1}{2}\sigma_1 [2, j] \right), \quad (\text{A.24a})$$

$$\gamma_{j+1} = (-1)^{j+1} \frac{1}{[1, 0]} \left([4, j] - \frac{1}{2}\sigma_1 [3, j] + \frac{1}{2} \left(\sigma_2 - \frac{1}{4}\sigma_1^2 \right) [2, j] \right), \quad (\text{A.24b})$$

$j = 0, 1$, where

$$[i, j] = \det \begin{pmatrix} I_1^i & I_1^j \\ I_2^i & I_2^j \end{pmatrix}. \quad (\text{A.24c})$$

In our case, thanks to the symmetry of the initial datum for the invariants, Eqs. (A.13) give $\sigma_1 = 0$ and $\sigma_2 = -r_4^2 - r_5^2 - r_6^2 = (-3u_0^2 + 4u_0q_0 - 12q_0^2) + 2(u_0 - 2q_0)\varepsilon - \varepsilon^2$. Upon making the substitutions $z = r_3 +$

$(r_4 - r_3) \sin^2 \theta$ on I_1^k and $z = r_5 + (r_6 - r_5) \sin^2 \theta$ on I_2^k and using the reflective symmetry of the initial datum, the integrals $I_{1,2}^0, \dots, I_{1,2}^4$ take the form:

$$I_1^k = (-1)^k r_4^k \int_0^{\pi/2} \frac{\cos^{2k} 2\theta}{\sqrt{(r_5^2 - r_4^2 \cos^2 2\theta)(r_6^2 - r_4^2 \cos^2 2\theta)}} d\theta, \quad (\text{A.25a})$$

$$I_2^k = \int_0^{\pi/2} \frac{(r_5 + \Delta \sin^2 \theta)^k}{\sqrt{(r_5 - r_4 + \Delta \sin^2 \theta)(r_4 + r_5 + \Delta \sin^2 \theta)(2r_5 + \Delta \sin^2 \theta)(r_5 + r_6 + \Delta \sin^2 \theta)}} d\theta, \quad (\text{A.25b})$$

where $\Delta = r_6 - r_5$. Then, evaluating the above integrals, substituting Eq. (A.25) and Eq. (A.24) into Eq. (A.17) and taking the limit $\varepsilon \rightarrow 0^+$, one then obtains the desired result, namely Eq. (3.2). Again, note that even though some of the integrals are divergent in the limit $\varepsilon \rightarrow 0^+$, the result for the characteristic speeds is finite.

Again, we emphasize that, by rescaling $q_0 \rightarrow q_0 + \frac{1}{2}u_0$ and $u_0 \rightarrow 2u_0$, the above calculation also provides both of the speeds $s_{\text{inner}}^{(1)}$ and $s_{\text{inner}}^{(2)}$ in Eq. (4.7) of section 4. More precisely, it is easy to see that, upon neglecting degenerate branches in Figs. 4.1b–d, the values of the Riemann invariants that determine s_5^+ in Fig. 3.2b are the same as those that determine s_9^+ in Fig. 4.1b–c $q_0 \rightarrow q_0 + \frac{1}{2}u_0$. Similarly, upon neglecting degenerate branches Figs. 4.1b–d one sees that the values that determine s_5^+ in Fig. 3.2b also coincide with those that determine s_7^+ in Fig. 4.1b and s_5^+ in Fig. 4.1c upon $u_0 \rightarrow 2u_0$.

References

1. M. J. Ablowitz and G. Biondini, “Multiple scale dynamics in communication systems with strong dispersion management”, *Opt. Lett.* **23**, 1668–1670 (1998)
2. M. J. Ablowitz and H. Segur, *Solitons and the Inverse Scattering Transform* (Society for Industrial and Applied Mathematics, Philadelphia, 1981)
3. M. Abramowitz and I. A. Stegun, *Handbook of mathematical functions* (Dover, New York, 1972)
4. G. P. Agrawal, *Nonlinear Fiber Optics* (Academic Press, San Diego, 1995)
5. E. D. Belokolos, A. I. Bobenko, V. Z. Enolskii, A. R. Its and V. B. Matveev, *Algebro-geometric approach to nonlinear integrable equations* (Springer, New York, 1994)
6. A. M. Bloch and Y. Kodama, “The Whitham equation and shocks in the Toda lattice”, 1–19, in *Singular limits of dispersive waves*, N. M. Ercolani, I. R. Gabitov, C. D. Levermore and D. Serre Eds., (Plenum, New York, 1994)
7. A. M. Bloch and Y. Kodama, “Dispersive regularization of the Whitham equation for the Toda lattice”, *SIAM J. Appl. Math.* **52**, 909–928 (1992)
8. J. D. Carter and H. Segur, “Instabilities in the two-dimensional cubic nonlinear Schrödinger equation”, *Phys. Rev. E* **68**, 045601 (2003)
9. G. A. El and A. L. Krylov, “General solution of the Cauchy problem for the defocusing NLS equation in the Whitham limit”, *Phys. Lett. A* **203**, 77–82 (1995)
10. G. A. El, V. V. Geogjaev, A. V. Gurevich and A. L. Krylov, “Decay of an initial discontinuity in the defocusing NLS hierarchy”, *Phys. D* **87**, 186–192 (1995)
11. T. J. Ellingham, J. D. Ania-Castañón, R. Ibbotson, X. Chen, L. Zhang and S. K. Turitsyn, “Quasi-lossless optical links for broadband transmission and data processing”, *Photon. Technol. Lett.*, to appear.

12. H. Flaschka, M. G. Forest and D. W. McLaughlin, "Multiphase Averaging and the Inverse Spectral Solution of the Korteweg-de Vries Equation", *Comm. Pure and Appl. Math.* **33**, 739-784 (1980).
13. M. G. Forest and J.-E. Lee, "Geometry and modulation theory for periodic nonlinear Schrödinger equation", in *Oscillation theory, Computation and Methods of Compensated Compactness*, IMA Vol. Appl. Math. **2**, Ed. C. Dafermos et alii (Springer, New York, 1986)
14. M. G. Forest and K. T.-R. McLaughlin, "Onset of oscillations in nonsoliton pulses in nonlinear dispersive fibers", *J. Nonlin. Sci.* **7**, 43-62 (1998)
15. I. R. Gabitov and S. K. Turitsyn, "Averaged pulse dynamics in a cascaded transmission system with passive dispersion compensation", *Opt. Lett.* **21**, 327-329 (1996)
16. F. Gesztesy and H. Holden, *Soliton equations and their algebro-geometric solutions* (Cambridge University Press, Cambridge, 2003)
17. T. Grava and F.-R. Tian, "The generation, propagation, and extinction of multiphases in the KdV zero-dispersion limit", *Commun. Pure Appl. Math.* **55**, 1569-1639 (2002)
18. H. Hammack, N. Scheffner and H. Segur, "Two-dimensional periodic waves in shallow water", *J. Fluid Mech.* **209**, 567-589 (1989)
19. A. Hasegawa and Y. Kodama, "The guiding-center soliton", *Phys. Rev. Lett.* **66**, 161-164 (1991)
20. A. Hasegawa and Y. Kodama, "The guiding-center soliton in fibers with periodically varying dispersion", *Opt. Lett.* **16**, 1385-1387 (1991)
21. A. Hasegawa and Y. Kodama, *Solitons in Optical Communications* (Oxford University Press, Oxford, 1995)
22. S. Jin, C. D. Levermore and D. W. McLaughlin, "The semiclassical limit of the defocusing NLS hierarchy", *Commun. Pure Appl. Math.* **52**, 613-654 (1999)
23. A. M. Kamchatnov, "New approach to periodic solutions of integrable equations and nonlinear theory of modulational instability", *Phys. Rep.* **286**, 199-270 (1997)
24. A. M. Kamchatnov, *Nonlinear periodic waves and their modulations: An introductory course* (World Scientific, New York, 2000)
25. Y. Kodama, "The Whitham equations for optical communications: mathematical theory of NRZ", *SIAM J. Appl. Math.* **59**, 2162-2192 (1999)
26. Y. Kodama and S. Wabnitz, "Analytical theory of guiding-center NRZ and RZ signal transmission in normally dispersive nonlinear optical fibers", *Opt. Lett.* **20**, 2291-2293 (1995)
27. I. M. Krichever, "Method of averaging for two-dimensional integrable equations", *Funct. Anal. Appl.* **22**, 37-52 (1988)
28. C. D. Levermore, "The hyperbolic nature of the zero dispersion limit of the KdV equation", *Commun. Partial Differential Equations* **13**, 495-514 (1988)
29. M. V. Pavlov, "Nonlinear Schrödinger equation and the Bogolyubov-Whitham method of averaging", *Theoret. Math. Phys.* **71**, 584-588 (1987)
30. F.-R. Tian, private communication
31. F.-R. Tian and J. Ye, "On the Whitham equations for the semiclassical limit of the defocusing nonlinear Schrödinger equation", *Commun. Pure Appl. Math.* **52**, 655-692 (1999)
32. F.-R. Tian and J. Ye, "On the breaking of the single-phase Whitham solution", *Phys. Lett. A* **277**, 115-119 (2000)
33. G. B. Whitham, "A general approach to linear and nonlinear dispersive waves using a Lagrangian", *J. Fluid Mech.* **22**, 273-283 (1965)
34. G. B. Whitham, *Linear and nonlinear waves* (Wiley, New York, 1974)

35. V. E. Zakharov and A. B. Shabat, “Exact theory of two-dimensional self-focusing and one-dimensional self-modulation of waves in nonlinear media”, *Sov. Phys. JETP* **34**, 62–69 (1972)